Published June 10, 2013

The netrin receptor DCC focuses invadopodia-driven basement membrane transmigration in vivo

Elliott J. Hagedorn,[1] Joshua W. Ziel,[1] Meghan A. Morrissey,[1] Lara M. Linden,[1] Zheng Wang,[1] Qiuyi Chi,[1] Sam A. Johnson,[1,2] and David R. Sherwood[1]

[1]Department of Biology, Duke University, Durham, NC 27708
[2]Light Microscopy Core Facility, Duke University and Duke University Medical Center, Durham, NC 27708

Though critical to normal development and cancer metastasis, how cells traverse basement membranes is poorly understood. A central impediment has been the challenge of visualizing invasive cell interactions with basement membrane in vivo. By developing live-cell imaging methods to follow anchor cell (AC) invasion in *Caenorhabditis elegans*, we identify F-actin–based invadopodia that breach basement membrane. When an invadopodium penetrates basement membrane, it rapidly transitions into a stable invasive process that expands the breach and crosses into the vulval tissue. We find that the netrin receptor UNC-40 (DCC) specifically enriches at the site of basement membrane breach and that activation by UNC-6 (netrin) directs focused F-actin formation, generating the invasive protrusion and the cessation of invadopodia. Using optical highlighting of basement membrane components, we further demonstrate that rather than relying solely on proteolytic dissolution, the AC's protrusion physically displaces basement membrane. These studies reveal an UNC-40–mediated morphogenetic transition at the cell–basement membrane interface that directs invading cells across basement membrane barriers.

Introduction

Basement membrane is a thin, dense, extracellular matrix that surrounds most tissues, acting as a physiological barrier to maintain tissue homeostasis (Kalluri, 2003). Several cell types, including those undergoing epithelial–mesenchymal transition, migrating neural crest and muscle, implanting trophoblast, and leukocytes have the specialized ability to breach and cross basement membrane barriers (Hughes and Blau, 1990; Poelmann et al., 1990; Sato et al., 2003; Wang et al., 2006; Nakaya et al., 2008). Acquisition of cell-invasive activity is also critical for the deadly spread of most cancers (Valastyan and Weinberg, 2011). Traversing basement membrane requires several distinct cellular processes, including matrix adhesion, basement membrane breaching and removal, passage through the basement membrane barrier, and integration into the neighboring tissue. The difficulty of visualizing and experimentally examining cell–basement membrane interactions during invasion in vivo has greatly limited our understanding of how cells coordinate these tasks during basement membrane transmigration (Rowe and Weiss, 2008; Madsen and Sahai, 2010).

Anchor cell (AC) invasion in *Caenorhabditis elegans* is a simple in vivo model of basement membrane transmigration that allows visual access to the invasive cell–basement membrane interface (Sherwood and Sternberg, 2003; Hagedorn and Sherwood, 2011). During normal hermaphrodite development, the uterine AC breaches the basement membrane separating the uterine and vulval epithelium to establish the initial connection between these tissues. The timing of AC invasion is highly stereotyped and is tightly coordinated with the division of the underlying vulval cells (Fig. S1 A). Both the integrin heterodimer INA-1/PAT-3 and the netrin receptor UNC-40 (DCC) localize to the cell membrane of the AC in contact with the basement membrane and are thought to promote invasion by regulating F-actin polarized toward the AC–basement membrane interface (Hagedorn et al., 2009; Ziel et al., 2009). How these pathways specifically mediate F-actin dynamics and facilitate basement membrane breaching and transmigration is unclear.

Correspondence to David Sherwood: david.sherwood@duke.edu

E.J. Hagedorn's present address is Boston Children's Hospital, Boston, MA 02115.

J.W. Ziel's present address is Skirball Institute of Biomolecular Medicine, New York University Medical Center, New York, NY 10016.

Abbreviations used in this paper: AC, anchor cell; PI(4,5)P_2, phosphatidylinositol 4,5-bisphosphate; VNC, ventral nerve cord.

This article is distributed under the terms of an Attribution–Noncommercial–Share Alike–No Mirror Sites license for the first six months after the publication date (see http://www.rupress.org/terms). After six months it is available under a Creative Commons License (Attribution–Noncommercial–Share Alike 3.0 Unported license, as described at http://creativecommons.org/licenses/by-nc-sa/3.0/).

Supplemental Material can be found at:
/content/suppl/2013/06/10/jcb.201301091.DC1.html
/content/suppl/2013/06/11/jcb.201301091.DC2.html
/content/suppl/2013/06/11/jcb.201301091.DC3.html

The Rockefeller University Press $30.00
J. Cell Biol. Vol. 201 No. 6 903–913
www.jcb.org/cgi/doi/10.1083/jcb.201301091

THE JOURNAL OF CELL BIOLOGY

Downloaded from on June 27, 2017

Published June 10, 2013

By developing methods for time-lapse microscopy of AC invasion, we identify here highly dynamic, integrin-dependent, F-actin–based structures that breach the basement membrane. These protrusive, F-actin–rich foci share molecular composition and activity with invadopodia, invasive structures identified in transformed and highly invasive cancer cells in vitro (David-Pfeuty and Singer, 1980; Chen, 1989; Murphy and Courtneidge, 2011). Many invadopodia form and turn over within the AC before invasion, but usually only one penetrates the basement membrane and then gives rise to a stable protrusion that invades the vulval tissue. We find that the netrin receptor UNC-40 (DCC) is highly enriched at sites of basement membrane breach and within the invasive protrusion. Animals lacking UNC-40 fail to form an invasive protrusion and have persistent invadopodia, multiple basement membrane breaches, and inefficient basement membrane removal. Using optical highlighting of basement membrane components, we show that this UNC-40–dependent invasive protrusion accelerates basement membrane removal in part by physically displacing this barrier. Together, these studies reveal an UNC-40 (DCC)–dependent mechanism that ensures focused invasion at nascent sites of basement membrane breach.

Results

Dynamic F-actin–based AC-invadopodia breach the basement membrane

To investigate how the AC crosses the basement membrane, we developed methods combining nontoxic anesthesia, multidimensional time-lapse microscopy, and quantitative image analysis to view the invasive cell–basement membrane interface in real time (Fig. 1 A and Video 1). Actin dynamics and basement membrane integrity were simultaneously visualized using animals expressing AC-specific F-actin probes (*cdh-3 > mCherry::moeABD* or *cdh-3 > Lifeact::GFP*) and functional transgenes for the basement membrane components laminin (*laminin::GFP*) and type IV collagen (*emb-9::mCherry*; Ziel et al., 2009; Ihara et al., 2011). Beginning 3 h before invasion, F-actin within the AC was polarized toward the basement membrane and organized into highly dynamic punctate structures with lifetimes on a timescale of minutes (Fig. 1 B; Fig. S1, B and E; and Video 1). Quantitative image analysis revealed these F-actin foci had a mean diameter of 1.00 ± 0.38 µm (±SD, n = 8,182 structures from 10 animals) and a median lifetime of 45 s (ranging from 15 to 930 s). Before invasion, nascent structures formed at a steady rate of 2.8 ± 0.4 structures per minute and there were on average 11 ± 3 structures present (Fig. S1 E).

F-actin–rich, matrix-degrading membrane structures called invadopodia have been identified in a variety of malignant cancer cell lines, as well as transformed fibroblasts and zebrafish epithelial cells (Linder et al., 2011; Murphy and Courtneidge, 2011; Seiler et al., 2012). Invadopodia are defined by their localization at sites of extracellular matrix removal, association with invasive cells, and highly protrusive nature (Linder et al., 2011; Murphy and Courtneidge, 2011). To determine if the F-actin structures in the AC were similar to invadopodia, we first examined their relationship to the basement membrane. High-resolution lateral perspective imaging at single time points revealed that these F-actin foci were highly protrusive, often appearing to depress the underlying basement membrane (Fig. 1 C and see Materials and methods). Time-lapse imaging from the ventral perspective showed that these structures always presaged and then localized to the site of the initial visible basement membrane breach (Fig. 1, D and E; Fig. S1 C; and Video 2; n = 8/8 animals observed). Strikingly, in most cases only one or two basement membrane breaches were made within a narrow 15-min period during the mid-to-late L3 larval stage (n = 6/12 animals had one breach, 3/12 two, 1/12 three, and 2/12 four; Fig. 2 C), usually occurring within the central region of the AC's footprint (Fig. S1 D). The protrusive nature of these F-actin structures and their localization at sites of basement membrane breach strongly suggest these are in vivo invadopodia.

Although there is no single molecular marker of invadopodia, many actin regulators are known to associate with these structures (Saltel et al., 2011; Klemke, 2012). We recently demonstrated that several actin regulators that are connected with invadopodia in vitro localize to the invasive cell membrane of the AC before invasion (Ziel et al., 2009). These include the Ena/VASP orthologue UNC-34, the phospholipid phosphatidylinositol 4,5-bisphosphate ($PI(4,5)P_2$), and the Rac GTPases MIG-2 and CED-10 (Nakahara et al., 2003; Philippar et al., 2008). Quantitative analysis revealed that all of these molecules colocalized with the F-actin foci in the AC (Fig. S2 A). Importantly, the cell membrane marker FM1-43 was found uniformly in the AC's invasive cell membrane, indicating that these structures are specific molecular enrichments as opposed to general accumulations of membrane (Fig. S2 B). In vitro studies have also demonstrated that engagement of the extracellular matrix receptor integrin is a prerequisite for invadopodia formation (Destaing et al., 2010). Notably, RNAi-mediated depletion of the integrin heterodimer INA-1/PAT-3, the sole integrin expressed in the AC (Hagedorn et al., 2009), dramatically reduced F-actin structure formation (Fig. S2 C; n = 8/8 animals). Collectively our results offer compelling evidence that these F-actin foci are AC-invadopodia.

An invadopodia-to-invasive protrusion transition drives the AC through a single basement membrane breach and into the vulval tissue

To determine how AC-invadopodia contribute to basement membrane transmigration, we followed the fate of the invadopodia that breached the basement membrane. We found that soon after breaching, an infiltrated invadopodium matured into an invasive process that expanded through the basement membrane and into the underlying vulval tissue (over an ∼1-h time frame and at a rate of 1.08 ± 0.42 μm^3/min; Fig. 2, A and C; and Video 3; n = 13 animals observed). At the onset of protrusion extension, AC-invadopodia ceased to form and F-actin enriched in the expanding cellular process (Video 4; n = 18/18 animals). As the invasive protrusion expanded ventrally, the corresponding breach widened radially until the completion of invasion (rate of 0.20 ± 0.06 μm^2/min; Fig. 2, B and C; and http://www.jcb.org/cgi/content/full/jcb.201301091/DC1Video 4; n = 13 animals). During this time the neck of the invading cellular protrusion

Downloaded from on June 27, 2017

Published June 10, 2013

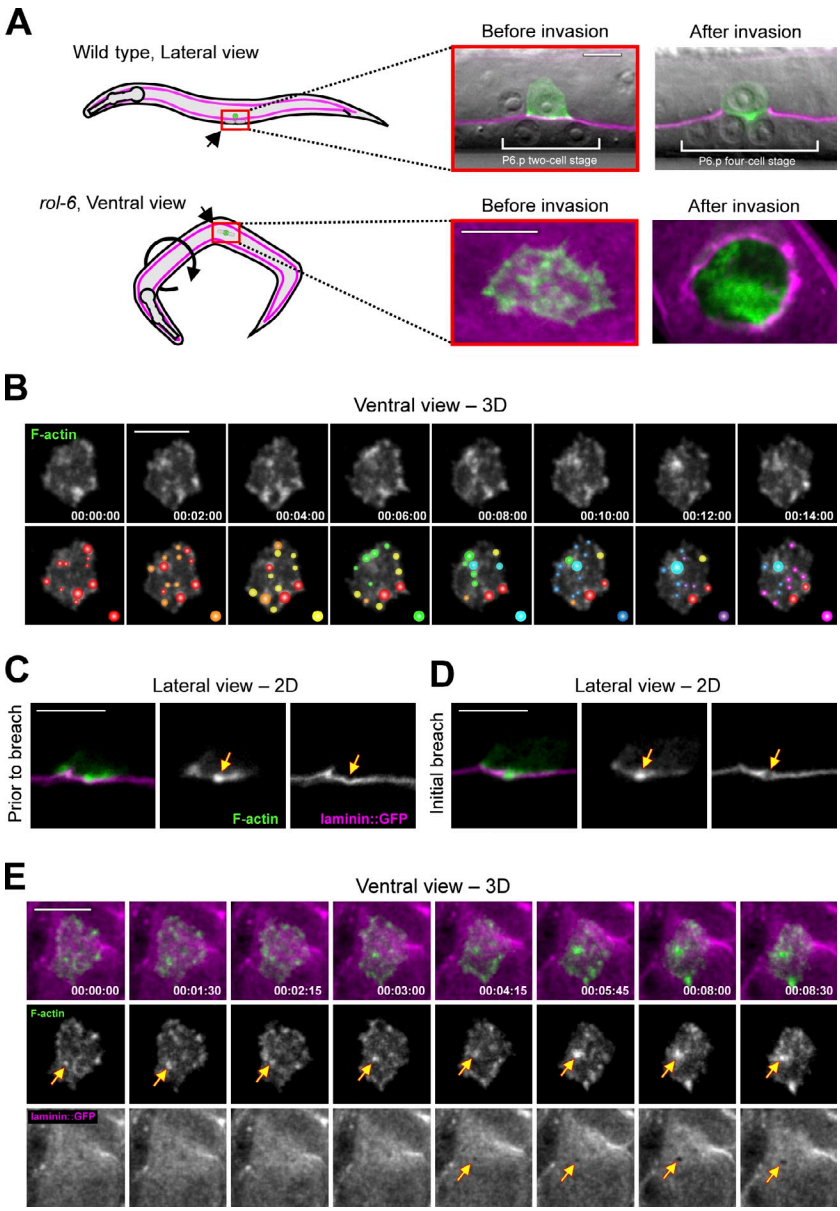

Figure 1. **F-actin–rich AC-invadopodia breach the basement membrane.** (A) A schematic diagram depicts the two perspectives used for time-lapse imaging of AC invasion. (top) Wild-type animals lay on their side, allowing AC invasion to be imaged laterally. The basement membrane is visualized with laminin::GFP in magenta and the AC-specific F-actin probe *cdh-3* > *mCherry::moeABD* is shown in green and overlaid on differential interference contrast images. (bottom) *rol-6* mutant animals orient randomly, permitting ventral imaging. Confocal slices through the AC–basement membrane interface are shown at magnification of two relative to top panels. Orientation is indicated in all panels. (B) Ventral view time series shows dynamic patches of F-actin–rich invadopodia at the AC–basement membrane interface. To illustrate the rapid rate of turnover, colored spots were assigned to new F-actin structures at 2-min intervals (see Fig. S1 for detailed information on size, lifetime, rate of formation, and number of invadopodia over time). The behavior of these F-actin structures was similar when visualized with Lifeact::GFP and when worms were immobilized by compression (Fig. S1). (C) Before breaching, invadopodia (middle, arrow) appear to depress the basement membrane (right, arrow). (D) At the time of basement membrane breach an invadopodium (middle, arrow) occupies the site of breach (right, arrow). (E) A ventral view time series shows an AC-invadopodium (middle row, arrows) presaging and then occupying a visible basement membrane breach (bottom, arrows; similar results were observed in 8/8 animals). Bars, 5 µm.

maintained contact with the basement membrane. In instances where two invadopodia breached, only one of these developed into a protrusion (n = 3/3 cases observed) that invaded the vulval tissue and widened a single large gap in the basement membrane (Fig. 2 B). Thus, when more than one invadopodia penetrates the basement membrane, a competitive interaction occurs between these sites, which results in a single invasive protrusion forming. Similar results were obtained examining the basement membrane component type IV collagen. Together, these results indicate that AC-invadopodia usually breach the basement membrane at only one or two sites and that only one invasive protrusion forms that directs invasion through the basement membrane and into the underlying vulval cells.

UNC-40 (DCC) enriches at sites of basement membrane breach

The observation that hundreds of invadopodia form and turn over before invasion, but only one or two basement membrane breaches form, suggested that a molecular signal might specify or reinforce the site of basement membrane breach. We have previously shown that UNC-6 (netrin) secreted from the ventral nerve cord (VNC) adjacent to the vulval cells promotes AC invasion, in part, by targeting its receptor UNC-40 (DCC) to the invasive cell membrane (Fig. S1 A; Ziel et al., 2009). To determine whether netrin signaling might select a site for basement membrane breach, we examined the localization of a functional GFP fusion to the netrin receptor UNC-40 (DCC). UNC-40::GFP was present throughout the invasive cell membrane before invasion, but did not tightly colocalize with the AC-invadopodia (Fig. S3 A). Consistent with this localization, loss of *unc-40* did not alter invadopodia formation or their dynamics before invasion (Fig. S3, B and C). Strikingly, however, UNC-40 enriched at nascent basement membrane breaches (Fig. 3, A and B; and Video 5). This enrichment in UNC-40 occurred ∼20 min before the formation of a visible basement membrane break, suggesting UNC-40 might promote basement membrane opening (Fig. 3 B).

Downloaded from on June 27, 2017

Published June 10, 2013

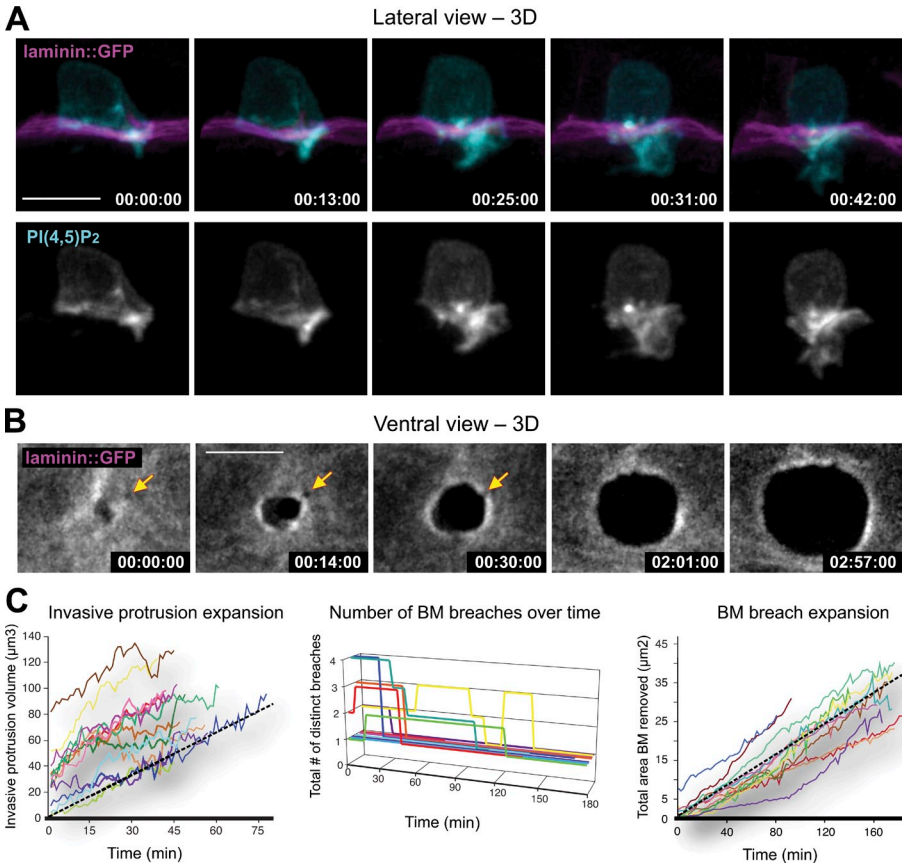

Figure 2. **Invadopodia give rise to an invasive protrusion that removes basement membrane.** (A) A lateral view time series shows the growth of the invasive membrane protrusion (viewed with the AC-specific PI(4,5)P_2 probe *cdh-3* > *mCherry*::PLCδ^{PH} in cyan [top; grayscale, bottom]) as it advances through the basement membrane (viewed with laminin::GFP in magenta [top]) and into the vulval epithelium. (B) A ventral view time series shows the expanding hole in the basement membrane that forms during AC invasion. The yellow arrows indicate a second breach that is overcome by the expanding basement membrane gap opening where the invasive protrusion is growing. Bars, 5 µm. (C) The graphs display the growth rate of the invasive protrusion (left) and dynamics of basement membrane gap formation (middle and right). Black dotted lines represent the mean rate of invasive protrusion expansion (1.08 ± 0.42 μm^3/min [±SD], mean r^2 = 0.83, n = 13) and basement membrane hole expansion (0.20 ± 0.06 μm^2/min [±SD], mean r^2 = 0.97, n = 13).

Supporting this notion, we found that in *unc-40 (e271)* mutant animals the initial visible breach was delayed by ∼1.5 h (Fig. 3 C). We conclude that UNC-40 (DCC) does not regulate invadopodia formation or dynamics, but has a role in promoting visible basement membrane gap formation.

UNC-40 (DCC) mediates invasive protrusion formation

The specific localization of UNC-40::GFP at sites of basement membrane breach led us to investigate the role of UNC-40 in building the stable invasive protrusion that forms shortly after basement membrane penetration. Notably, UNC-40::GFP continued to further enrich during basement membrane opening and localized to the invasive process that extended into the vulval tissue (Fig. 3 B and Fig. S4 A). This specific enrichment suggested that UNC-40 might promote basement membrane opening and the transition of invadopodia into an invasive process that switches the invasive state of the AC from invadopodia-driven basement membrane breaching to invasive protrusion-directed basement membrane crossing. Consistent with this idea, though delayed in breaching, in *unc-40* mutant animals the invadopodia persisted after visible basement membrane gaps were formed, often resulting in excessive breaches (as many as seven; Fig. 4, A and B; and Fig. S4 B). Furthermore, we never observed the formation of a significant invasive protrusion after loss of *unc-40* (Fig. 4, C and D). The hole in the basement membrane of *unc-40* mutant animals widened at half the rate of wild-type animals (Fig. 4, E and F; and Video 6), suggesting that the protrusion is important for basement membrane gap opening. Collectively, these data indicate that UNC-40 mediates a morphogenetic transition that promotes the maturation of an invadopodium into a stable invasive protrusion, which leads to the cessation of further invadopodia formation, invasion into the neighboring vulval tissue, and accelerated basement membrane removal.

UNC-40 activity is dependent on UNC-6 during invadopodia maturation

We next examined the relationship between UNC-40 and UNC-6 during invadopodia maturation. UNC-6 is secreted from the VNC adjacent to the vulval cells, and we have previously shown that low, uniform levels of the functional reporter UNC-6::Venus are present in the basement membrane at the time of invasion (Ziel et al., 2009). We found that *unc-6 (ev400)* mutants displayed a phenotype largely similar to loss of *unc-40*—there was a delay in basement membrane breaching, a multiple basement membrane hole phenotype, and a complete failure to extend an invasive protrusion through the basement membrane (Fig. 4, A–D). Notably, the multiple basement membrane hole phenotype was more severe in *unc-40* mutants, suggesting that this activity is not fully dependent on UNC-6 (Fig. 4 B). Examination of UNC-40::GFP in *unc-6 (ev400)* mutants also revealed that UNC-40::GFP still enriched at basement membrane breaches (Fig. S4 C). These observations suggest that UNC-6 activates the UNC-40 receptor, but that another mechanism must exist to selectively localize UNC-40 to the site of basement membrane breach.

Downloaded from on June 27, 2017

Published June 10, 2013

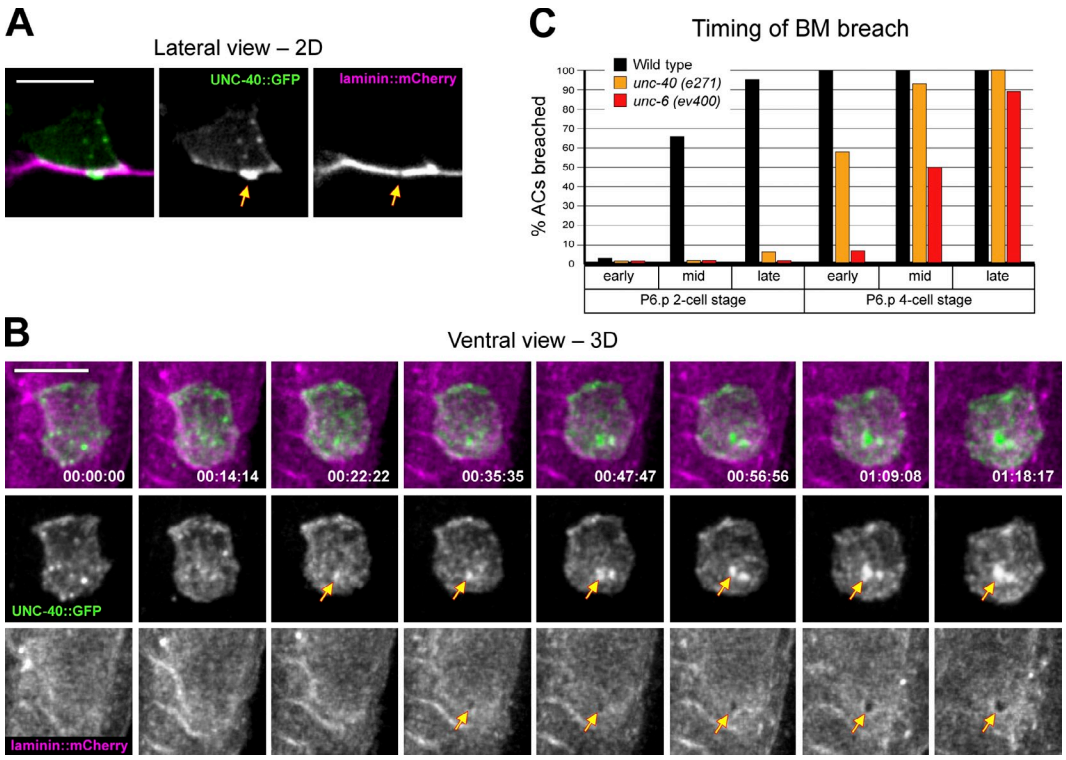

Figure 3. **UNC-40 (DCC) presages and then enriches at the basement membrane breach.** (A) The netrin receptor UNC-40::GFP (middle, arrow) enriches at the site of basement membrane breach (right, arrow). (B) A ventral view time series shows that UNC-40::GFP (middle row, arrows) presages and then progressively enriches at the basement membrane breach as it expands (bottom, arrows). (C) Timing of basement membrane breach in wild-type, *unc-40 (e271)*, and *unc-6 (ev400)* mutant animals ($n \geq 14$ animals observed for each genotype, at each time point). Timing was assigned in relationship to the divisions of the neighboring uterine and P6.p vulval cells (Fig. S1). The time between the mid P6.p two-cell stage when wild-type animals initiate breach and early P6.p four-cell stage when *unc-40* mutants penetrate basement membrane is ~1.5 h at 20°C. Bars, 5 µm.

UNC-40 effectors localize to basement membrane breaches and promote invasive protrusion formation

We next addressed how UNC-40 promotes formation of an invasive protrusion. UNC-40 (DCC) is thought to function in cell migration and axon guidance by recruiting and activating downstream effectors that modulate the actin cytoskeleton (Quinn et al., 2008; Ziel et al., 2009; Lai Wing Sun et al., 2011). We therefore examined the localization of functional GFP-tagged reporters for known UNC-40 effectors to determine if they are recruited to basement membrane breaches like UNC-40. We found that the Ena/VASP orthologue UNC-34 and the Rac orthologue MIG-2 both enriched at the initial basement membrane breach in wild-type animals but that this enhancement in localization was absent in *unc-40* mutants (Fig. 5 A and Fig. S4 D). Furthermore, examination of F-actin, the output of these effectors, revealed dynamic and focused formation at the expanding site of breach during protrusion growth with F-actin repeatedly forming and disassembling at the site of breach where UNC-40 was stably localized (Fig. 5, B and C; Video 7; and Video 8). In contrast, in *unc-40* mutant animals, dynamic F-actin polymerization was not focused at sites of breach (Fig. 5 C and Video 9). Consistent with these effectors acting downstream of UNC-40 at sites of basement membrane breach, we have previously reported that perturbation of these molecules leads to a delay in AC invasion (Ziel et al., 2009). To determine if these effectors might also mediate invasive protrusion formation, we examined *unc-34(e951); mig-2(mu28)* double mutant animals. Supporting a role in fostering invasive protrusion growth downstream of UNC-40, we found a complete absence of invasive processes after loss of *unc-34* and *mig-2* ($n = 9/9$ animals observed). These results suggest that UNC-40 directs focused F-actin generation through F-actin regulatory proteins at the site of basement membrane breach to direct stable protrusion formation.

The AC's invasive protrusion physically displaces basement membrane to widen the basement membrane gap

We were next interested in understanding how the UNC-40–mediated invadopodia-to-invasive protrusion transition enhances basement membrane removal. During our initial analysis, we noted that the invasive protrusion in wild-type animals remained in continuous contact with the edge of the expanding basement membrane gap (Fig. S5 A). Further, the basement membrane opening was much rounder in wild-type animals versus *unc-40* mutants, even in cases where only a single gap was created (Fig. 6, B and C; wild type: circularity = 0.89, $n = 15$; *unc-40(e271)*: circularity = 0.56, $n = 14$; $P < 0.0001$, Student's t test). Finally, we noticed increased levels of laminin and type IV collagen at the rim of the expanding basement membrane gap in wild-type animals (Fig. S5 B). These observations suggested that the expanding protrusion might speed basement membrane gap opening by physically displacing the basement membrane. Importantly, the AC is known to secrete matrix components during

Downloaded from on June 27, 2017

Published June 10, 2013

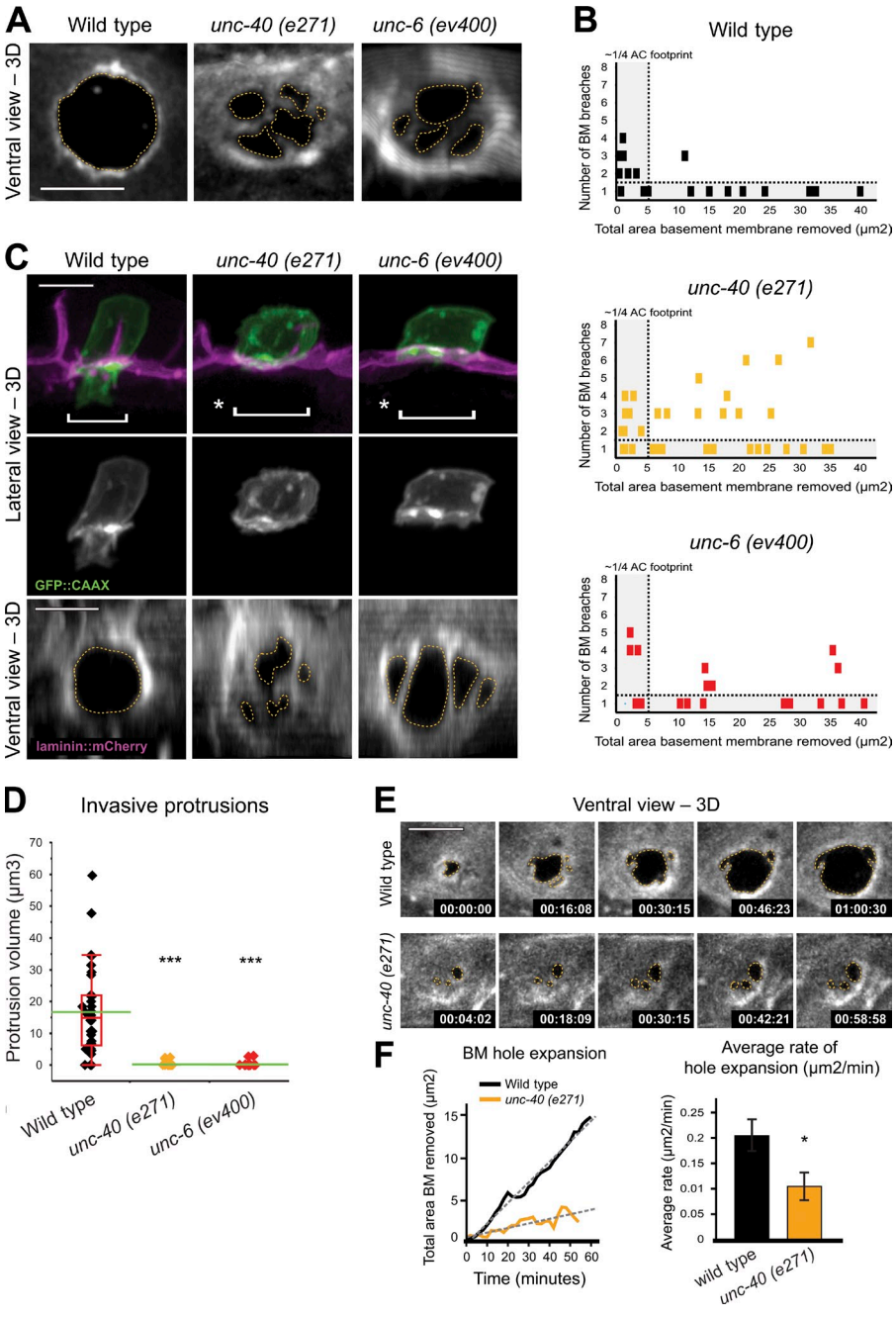

Figure 4. **UNC-40 and UNC-6 promote invasive protrusion formation and basement membrane clearance.** (A) A single basement membrane gap (basement membrane viewed with laminin::GFP) is formed in wild-type animals (left, outlined by dotted line), whereas in *unc-40* and *unc-6* mutants multiple basement membrane breaches occur (middle and right). (B) Quantification of basement membrane breaching (each block represents one animal) reveals that when multiple basement membrane breaching events occur in wild-type animals, they quickly resolve into a single gap (top). In contrast, when multiple breaches occur in *unc-40* and *unc-6* mutants they often fail to resolve into a single basement membrane hole (middle and bottom). (C) Examination of ACs expressing the cell membrane marker *cdh-3* > GFP::CAAX (top, green; middle, grayscale) reveals the presence of an invasive protrusion (bracket) that extends across the basement membrane (top left, magenta) through a single basement membrane gap in a wild-type animal (bottom left, ventral view, grayscale). In *unc-40* (middle) and *unc-6* (right) mutants no invasive protrusion is extended (asterisks with brackets) through the multiple basement membrane gaps (bottom). (D) Quantification of the volume of the invasive protrusion formed within an hour of initial basement membrane breach in wild-type, *unc-6*, and *unc-40* mutant animals ($n \geq 28$ animals examined for each genotype). The asterisks denote statistically significant differences ($P < 0.0001$, Wilcoxon rank-sum test). (E) A ventral view time series of the basement membrane (visualized with laminin::GFP) in a wild-type animal (top) captures the faster rate of basement membrane opening compared with an *unc-40* mutant (bottom; see Video 6). (F) The graphs show quantification of basement membrane removal over time for the animals shown in E (left) and the mean rates of hole expansion for wild-type and *unc-40(e271)* animals (right). Asterisk denotes a statistically significant difference ($P = 0.01$, Student's *t* test; $n = 6$ animals per genotype). Error bar represents SEM. Bars, 5 µm.

invasion (Sherwood et al., 2005), and so we could not exclude the possibility that this increase was simply a result of new basement membrane deposition. Thus, to directly test whether displacement was occurring we used transgenic animals expressing laminin::Dendra or type IV collagen::Dendra. Dendra is a highly stable, photoconvertible fluorescent protein that changes irreversibly from a green to a red fluorescent state after exposure to low phototoxic, short wavelength light (Gurskaya et al., 2006). To determine if the basement membrane was displaced during invasion, we optically highlighted the basement membrane precisely beneath the AC before invasion using an AC-specific GFP membrane marker (Fig. 6 A). We observed photoconverted laminin::Dendra displaced to the sides of the AC after invasion, nearly doubling the distance between the outer edges of highlighted region (Fig. 6, A and C), indicating that the basement membrane was physically moved. In contrast, control regions of optically highlighted basement membrane adjacent to the AC remained intact and only slightly widened, likely because of diffusion of basement membrane components and growth (the basement membrane beneath the AC widened 1.8- versus 1.2-fold in control regions; Fig. 6, A and C; Ihara et al., 2011). To quantify the amount of the basement membrane displaced during invasion, we photoconverted all of the laminin:Dendra in the vicinity of the AC before invasion. An estimate of the percentage of basement membrane displaced was then calculated based on the additional fluorescence intensity at the edges of the expanding gap (see Materials and methods; Fig. 6, B and C). Using this approach we determined that a

Downloaded from on June 27, 2017

Published June 10, 2013

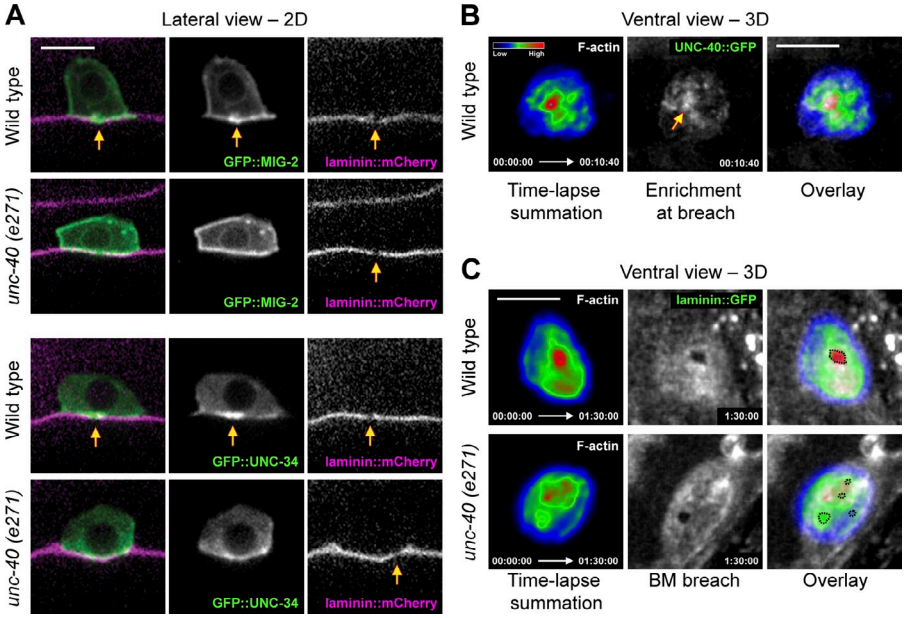

Figure 5. **UNC-40 directs F-actin formation at the site of protrusion formation.** (A) F-actin effectors (middle), basement membrane (right), and overlay (left) show that GFP::MIG-2 (Rac) and GFP::UNC-34 (Ena/VASP) localize to the initial site of basement membrane breach in wild-type animals (top, arrows) but fail to do so in *unc-40 (e271)* mutants (bottom, arrows). (B) The spectral representation of the fluorescence intensity of the summation of a 10-min, 40-s time-lapse shows that F-actin (left, viewed with *cdh-3* > mCherry::moeABD) overlaps precisely with the stable patch of UNC-40::GFP (middle, arrow; overlay right; see Video 7; similar results were observed in 6/6 animals). (C) A similar summation of a 90-min time-lapse revealed that this dynamic F-actin formation (top, left) was targeted at the site of invasive protrusion formation at the center of the basement membrane gap (middle, viewed with laminin::GFP) in a wild-type animal (see Video 8). In contrast, in *unc-40* mutants (bottom), F-actin was not concentrated at the sites of basement membrane breach (see Video 9). Bars, 5 µm.

mean of 26% of the basement membrane was physically displaced during AC invasion in wild-type animals (Fig. 6, B and C; $n = 27$). Importantly, this estimate likely underrepresents basement membrane displacement, as our method for quantification can only measure basement membrane that accumulated at the edge of the expanding gap and does not account for basement membrane that might be stretched thin or moved beyond the boundary of the basement membrane gap. Similar results were obtained with type IV collagen::Dendra (Fig. S5 C). In *unc-40 (e271)* mutants, where an invasive protrusion is never formed, we observed that only 8% of the basement membrane was displaced during gap formation ($n = 14$; $P = 0.0012$; Fig. 6, B and C), supporting the notion that the invasive protrusion in wild-type animals accelerates basement membrane removal by displacement. The finding that some laminin and type IV collagen still accumulate at the edges of basement membrane openings in *unc-40* mutants suggests that a redundant mechanism might also exist to physically move basement membrane or that basement membrane diffusion may facilitate displacement. We conclude that the invasive protrusion enhances basement membrane crossing, in part, by physically displacing this barrier to clear a path for invasion.

Discussion

The ability of cells to invade through basement membrane and enter new tissues is critical to many normal morphogenetic processes as well as cancer metastasis. By developing real-time methods to visualize AC invasion in *C. elegans*, we find that dynamic invadopodia are used to breach the basement membrane. Further, we show that the UNC-40 (DCC) receptor localizes to sites of basement membrane breach and directs the creation of a single large invasive protrusion that displaces basement membrane, guides invasion into the underlying vulval tissue, and leads to the cessation of further invadopodia formation (for a summary, see Fig. 7). Together, our results reveal a key UNC-40–mediated morphogenetic transition that directs invading cells through basement membrane and into neighboring tissues.

To date, invadopodia, defined primarily by their protrusive nature and ability to remodel extracellular matrix, have only been described in metastatic cancer cell lines or transformed cells (Chen, 1989; Linder et al., 2011; Seiler et al., 2012). Using live-cell imaging, we find that basement membrane breaching during AC invasion is mediated by protrusive F-actin–based invadopodia. Although most of the F-actin–based structures within the AC were similar in size and stability (~1 µm in diameter and lifetime of 45 s; Fig. S1 E), some were consistently outside of this range in dimension and lifetime. Thus, these F-actin foci are likely not all invadopodia and some may be sites of endocytosis and adhesion. Nevertheless, the largely similar dynamics and their striking disappearance shortly after basement membrane breaching offers compelling evidence that many if not most of these structures are bona fide in vivo invadopodia.

Over fifty proteins are known to localize to or regulate invadopodia function in cancer cells (Hoshino et al., 2012; Klemke, 2012). Our initial characterization indicates that the invadopodia in the AC have similar molecular composition to cancer cell invadopodia, including the presence of *C. elegans* orthologues of vertebrate Rac GTPases and Ena/VASP, as well as the presence of the phospholipid $PI(4,5)P_2$ (Nakahara et al., 2003; Philippar et al., 2008; Yamaguchi et al., 2010). The AC-invadopodia also share a dependency on integrin activity (Destaing et al., 2010). Additionally, the *C. elegans* genome encodes orthologues of many additional proteins implicated in invadopodia formation or function, such as the Src and FAK tyrosine kinases, paxillin, the Arp 2/3 complex, the actin nucleation-promoting factor WASP, and matrix metalloproteinases, which may play a similar role in the AC as they do in cancer cells (Saltel et al., 2011; Shaye and Greenwald, 2011; Hoshino et al., 2012; Klemke, 2012). One notable exception, however, is the absence of the actin nucleation–promoting factor cortactin in *C. elegans*, a key regulator of invadopodia in several cancer

Downloaded from on June 27, 2017

Published June 10, 2013

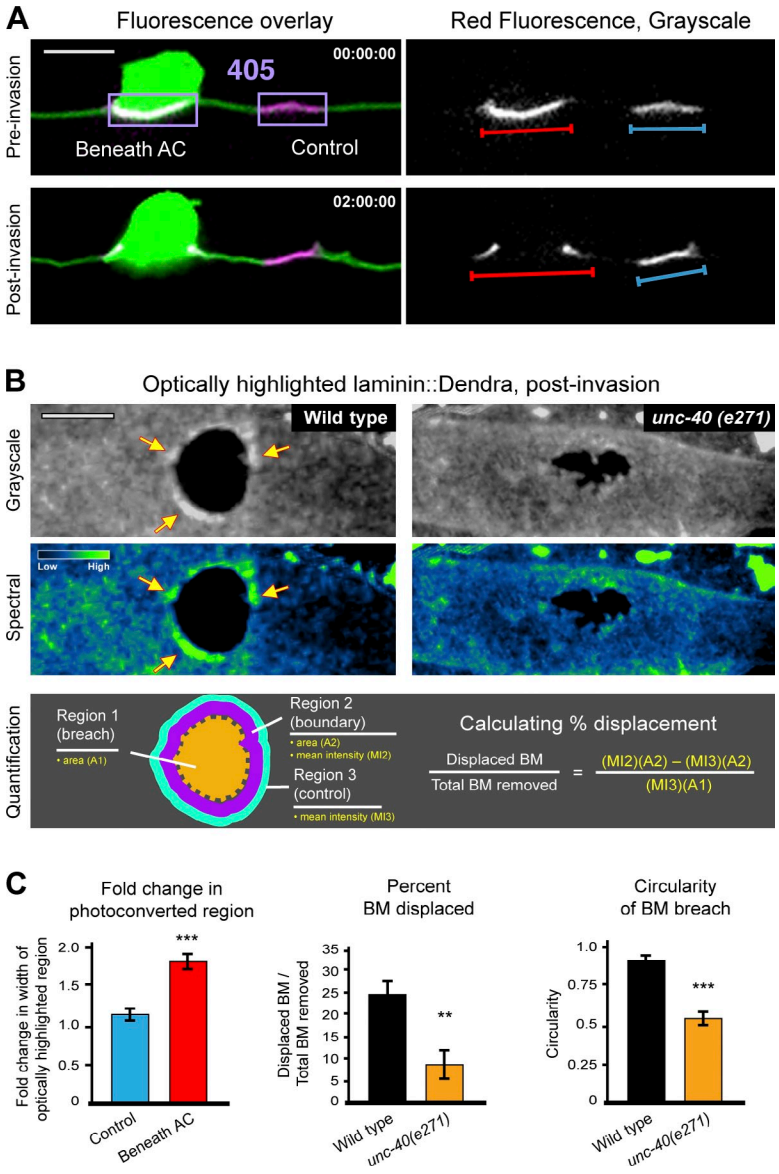

Figure 6. **The basement membrane is physically displaced by the UNC-40–generated invasive protrusion.** (A) Lateral view images show two regions of laminin::Dendra (one beneath the AC and an adjacent control) that were photoconverted by brief exposure to 405-nm light (left, fluorescence overlay; right, grayscale of red fluorescence). Only time points after photoconversion are shown. Cytoplasmic GFP expression (*cdh-3* > GFP) was used to precisely determine the boundaries of the AC's footprint. The same animal is shown before invasion (top) and 2 h later, after AC invasion (bottom). The region of photoconverted laminin:Dendra beneath the AC was displaced laterally during invasion (red bar) compared with the control region that remained unchanged (blue bar; quantification reported in C). (B) Ventral view images show grayscale (top) and corresponding spectral representation of fluorescence intensity (middle) of wild-type (left) and *unc-40(e271)* (right) animals in which the entire region shown was photoconverted before invasion. Only time points after invasion are shown. Yellow arrows point to accumulation of photoconverted laminin:Dendra at the boundary of the expanding breach. The schematic diagram (bottom) depicts the quantitative method used to estimate basement membrane displacement. (C) Graph displays the fold change in optically highlighted regions before and after invasion (left, see A [right] for corresponding measurements). Measurements of the percentage of basement membrane displaced (middle) and the circularity of basement membrane breaches (right and see Materials and methods) in wild-type and *unc-40(e271)* animals are reported. The asterisks denote statistically significant differences ($P < 0.001$, Student's *t* test; $n \geq 14$ animals for each genotype). Error bars represent SEM. Bars, 5 µm.

cell lines (Artym et al., 2006; Ayala et al., 2008; Shaye and Greenwald, 2011). Thus, the AC-invadopodia might have differences in their regulation and composition from cancer cells, or other proteins may compensate for the absence of cortactin in *C. elegans*.

We have also discovered that soon after an invadopodium penetrates the basement membrane, a large invasive protrusion forms at the site of breach and invades the underlying vulval epithelium. Formation of a stable protrusion is accompanied by the cessation of invadopodia, thus shutting down additional basement membrane breaches and focusing invasion through a single basement membrane gap. Transition to an invasive protrusion likely also stabilizes an invasion site by anchoring a cell to the neighboring tissue. Studies in ex vivo invasion assays have observed single protrusions from invasive cancer cells crossing native basement membrane (Hotary et al., 2006; Schoumacher et al., 2010), consistent with this being a conserved mode of basement membrane invasion. Importantly, we have found that the netrin ligand UNC-6 and its receptor UNC-40 (DCC) mediate this critical switch. UNC-40 selectively enriched at sites where invadopodia first visibly breached the basement membrane, and through activation by UNC-6 and recruitment of effectors, promoted F-actin formation and the construction of an invasive protrusion. Although netrins are well established for their role in mediating axon guidance, cell migration, and epithelial morphogenesis (Lai Wing Sun et al., 2011), they are also proangiogenic factors in vertebrates and promote vascular sprouting through basement membrane (Heissig et al., 2003; Wilson et al., 2006). Further, the netrin-1 ligand is overexpressed in numerous metastatic cancers (Fitamant et al., 2008; Dumartin et al., 2010; Ramesh et al., 2011) and stimulates invasion in pancreatic, colon, glioblastoma, and melanoma cancers assayed in vitro and ex vivo (Rodrigues et al., 2007; Kaufmann et al., 2009; Dumartin et al., 2010; Shimizu et al., 2012). These results suggest that netrin signaling broadly promotes invasion and that netrin might play a conserved role in directing invasive protrusion formation. Surprisingly, evidence in vertebrates and *Drosophila melanogaster* have suggested that UNC-40 (DCC) receptors

Downloaded from on June 27, 2017

Published June 10, 2013

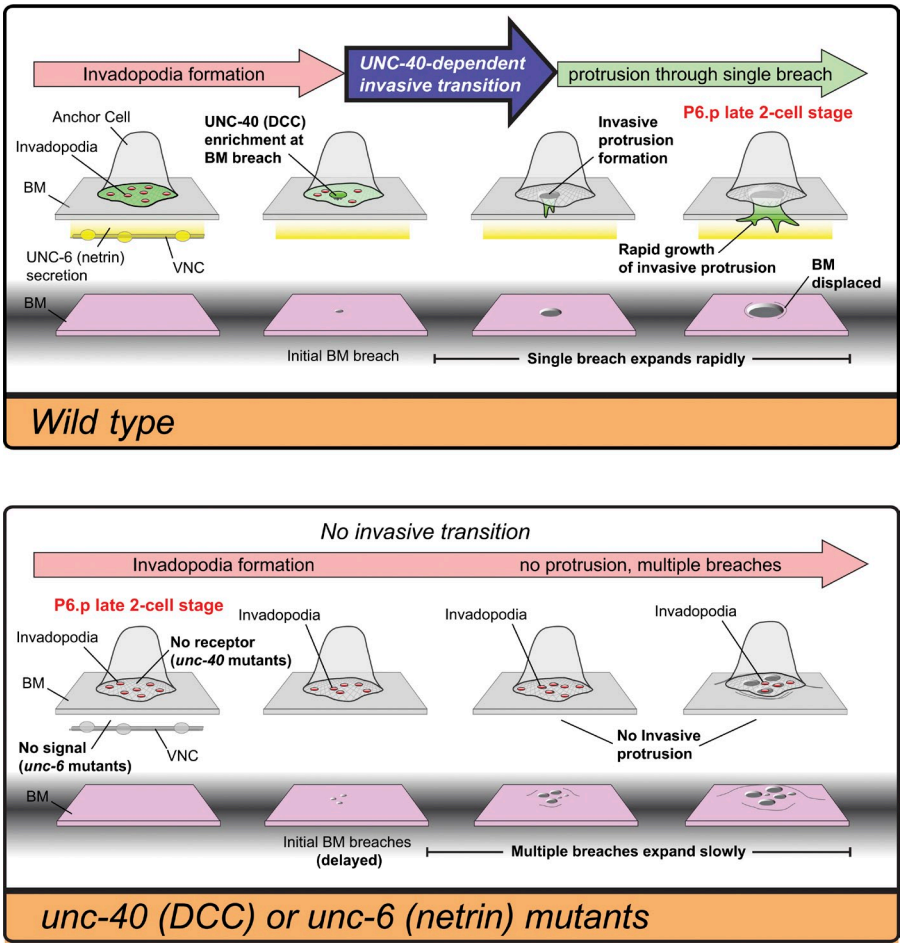

Figure 7. **The netrin receptor UNC-40 promotes invadopodia-to-invasive protrusion transition within the AC.** In wild-type animals (top) numerous invadopodia turn over before one penetrates the basement membrane. The UNC-40 (DCC) receptor enriches at the basement membrane breach and through its effectors generates F-actin that builds a large stable protrusion. This invasive process physically displaces basement membrane (BM) and directs invasion through a single basement membrane gap into the underlying vulval tissue. UNC-6 (netrin) secreted from the VNC activates UNC-40, but a distinct mechanism recruits UNC-40 to sites of basement membrane penetration. In the absence of UNC-40 signaling, invadopodia fail to transition into an invasive protrusion and invadopodia persist, generating multiple breaches that inefficiently clear gaps in the basement membrane.

may also function as tumor and metastasis suppressors, perhaps through their role in maintaining epithelial and endothelial cell survival in the presence of netrin ligands and promoting apoptosis in their absence (VanZomeren-Dohm et al., 2011; Castets et al., 2012; Krimpenfort et al., 2012). These observations indicate that in different cell contexts DCC may function as either a tumor suppressor or enhancer during cancer progression.

The expression of matrix-degrading proteases and the presence of type IV collagen degradation products at sites of invasion in human carcinomas have supported the widely held idea that basement membrane barriers are overcome through proteolytic dissolution by invasive cells (Garbisa et al., 1980; Xu et al., 2001; Sherwood et al., 2005; Hotary et al., 2006; Overall and Kleifeld, 2006; Page-McCaw et al., 2007). Intriguingly, studies of epithelial and carcinoma cells have shown that these cells physically compress and displace basement membrane components in vitro (Rabinovitz et al., 2001), a cellular behavior that might also contribute to creating gaps in endogenous basement membrane. Using optical highlighting, we found that the AC physically displaces the basement membrane components laminin and type IV collagen during basement membrane gap formation. Our quantitative analysis suggests that at least 26% of basement membrane is displaced during invasion. We think this is an underestimate, as our methods for determining displacement cannot account for basement membrane that stretches or moves beyond the basement membrane gap boundary. Notably, we previously found that the matrix metalloproteinase *zmp-1* is expressed in the AC during invasion, where it may act redundantly with other proteases that promote basement membrane removal (Sherwood et al., 2005). These results offer a new model to account for cell invasion through basement membrane barriers, where the combined action of proteases and physical forces coordinate basement membrane removal. Collectively our studies indicate that basement membrane transmigration is not a simple process of basement membrane dissolution, but rather a progressive series of highly regulated and interlinked steps that act to mediate breaching, removal, and passage through basement membrane barriers.

Materials and methods

Strains and culture conditions

Culturing and handling of *C. elegans* was done as previously described (Brenner, 1974). Wild-type animals were strain N2. In the text and figures, we designated linkage to a promoter with a greater than symbol (>) and used a double colon (::) for linkages that fuse open reading frames. The following alleles and transgenes were used in this study: *qyIs61[cdh-3 > GFP::UNC-34]*, *qyIs242[cdh-3 > Lifeact::GFP]*, *qyIs46[emb-9::mCherry]*, *qyIs221[cdh-3 > GFP::CED-10]*, *qyIs219[cdh-3 > GFP::PLCδ^{PH}]*, *qyIs220[cdh-3 > GFP::MIG-2]*, *qyIs67[cdh-3 > UNC-40::GFP]*, *qyIs127[laminin::mCherry]*, *qyIs166[cdh-3 > GFP::CAAX]*; LGI, *unc-40(e271)*; LGII, *qyIs23[cdh-3 > mCherry::PLCδ^{PH}]*; LGIII, *unc-119(ed4)*; LGIV, *qyIs10[laminin::GFP]*; LGV, *qyIs50[cdh-3 > mCherry::moeABD]*; and LGX, *qyIs7[laminin::GFP]*, *unc-6(ev400)*, *qyIs24[cdh-3 > mCherry::PLCδ^{PH}]*, and *qyIs66[cdh-3 > UNC-40::GFP]*.

Downloaded from on June 27, 2017

Published June 10, 2013

Microscopy, image acquisition, processing, and analysis

Images were acquired using a camera (EM-CCD; Hamamatsu Photonics) and a spinning disk confocal microscope (CSU-10; Yokogawa) mounted on a microscope (AxioImager; Carl Zeiss) with a Plan-APOCHROMAT 100×/1.4 oil differential interference contrast objective and controlled by iVision software (Biovision Technologies). Acquired images were processed using ImageJ 1.40g and Photoshop (CS3 Extended; Adobe). 3D reconstructions were built from confocal z-stacks, analyzed, and exported as .mov files using IMARIS 7.4 (Bitplane, Inc.). Figures and graphs were constructed using Illustrator (CS3 Extended; Adobe). Videos were annotated using Photoshop. Quantitative analyses of AC-invadopodia, invasive protrusion, or basement membrane breach formation was done using either ImageJ, Imaris, or both. To be as consistent as possible isosurface renderings, built in place of polymerized F-actin, were used to determine a threshold for assigning the spots that were used to quantify AC-invadopodia dynamics. For time-lapse microscopy, worms were anesthetized in 0.2% tricaine and 0.02% levamosile in M9 and then transferred to 5% noble agar pads, sealed with VALAP, and imaged at 23°C. Capturing the AC-invadopodia structures that presaged the initial basement membrane breach required ventral view time-lapse imaging. Although AC-invadopodia could be observed to depress the basement membrane in single time point lateral view images, we were unable to resolve whether the structures that presaged the initial breach repeatedly depressed the basement membrane.

RNAi

RNAi targeting *pat-3* was delivered by feeding worms *Escherichia coli* expressing double-stranded RNA. To avoid embryonic lethality, synchronized L1-arrested larvae were grown for 5 h on regular OP50 bacteria in the absence of RNAi. These worms were then transferred to bacteria expressing *pat-3* double-stranded RNA. The empty RNAi vector L4440 was used as a negative control. The RNAi vector was sequenced to verify correct insert.

Construction of GFP protein fusions

Lifeact::GFP was amplified from pJWZ73, and then linked by PCR fusion to the *cdh-3* > promoter. MIG-2 and CED-10 were both amplified from N2 genomic DNA and then linked to a *cdh-3* > *GFP* amplicon by PCR fusion. The PLCδ^{PH} domain was amplified from pAA173, cloned into pBsSK at the C-terminus of GFP and then linked to the *cdh-3* > promoter and *unc-54* 3′UTR using a three-step PCR fusion. GFP::CAAX was amplified from pSA129, and then linked by PCR fusion to the *cdh-3* > promoter. Constructs were coinjected with ∼50 ng/µl *unc-119* rescue DNA, ∼50 ng/µl pBsSK, and ∼50 ng/µl EcoRI cut salmon sperm DNA into *unc-119(ed4)* hermaphrodites. Stably expressed extrachromosomal lines were established and selected lines were integrated by gamma irradiation. See Tables S1 and S2 for primer sequences used and transgenic strains generated.

Staining with the lipophilic dye FM1-43

To visualize the plasma membrane of the AC we used the lipophilic dye FM1-43, which fluoresces green when incorporated into the outer leaflet of the plasma membrane.

Approximately 25 wild-type N2 worms at the early L3 larval stage were transferred to 25 µl of a 0.5 mM FM1-43 dye in M9 in a well of a glass spot plate. The spot plate was covered with parafilm and placed in the dark for 1 h. After incubation, worms were allowed to destain on OP50 food plates for an additional hour. Worms were mounted on 5% noble agar pads containing 0.01 M sodium azide and imaged using a spinning disc confocal and 488-nm laser.

Optical highlighting (photoconversion) of basement membrane components

Defined regions of laminin::Dendra and type IV collagen::Dendra were photoconverted using a confocal microscope (LSM 510; Carl Zeiss) equipped with a 63× objective, scanning regions of interest with a 405-nm laser at 1 mW power for 30 s. After photoconversion, images were captured using a spinning disc confocal or an AxioImager microscope. Animals were recovered from the agar pad, allowed to develop at 20°C for the specified amount of time, and then reimaged. The fold change in width of the optically highlighted regions was measured using ImageJ 1.40g. Quantification of percent displacement was done by photoconverting all of the basement membrane within a 15-µm radius of the AC, recovering the worms for 2–3 h, and then reimaging from the ventral perspective. Sum projections of confocal z-stacks were then analyzed using ImageJ 1.40g software and the method described in Fig. 6 B. Measurements of circularity were performed by tracing the boundary of single basement membrane breaches in ImageJ and calculated as $4\pi(\text{area}/\text{perimeter}^2)$.

Statistical analysis

All statistical analysis was performed in JMP version 9.0 (SAS Institute), using either a two-tailed unpaired Student's *t* test or nonparametric Wilcoxon rank-sum test. Figure legends specify when each test was used.

Online supplemental material

Online supplemental material includes five figures, nine videos corresponding to the time-lapse data presented in the main text figures, and two tables, Table S1 for primer sequences and Table S2 for extrachromosomal arrays and integrated strains. Online supplemental material is available at http://www.jcb.org/cgi/content/full/jcb.201301091/DC1. Additional data are available in the JCB DataViewer at http://dx.doi.org/10.1083/jcb.201301091.dv.

We are grateful to the Duke University Light Microscopy Core Facility and P. Maddox for advice and reagents, to the Caenorhabditis Genetic Center for providing strains, to the staff at Bitplane, Inc. (Imaris) for technical support, and to L. Kelley and L. Lilley for comments on the manuscript.

This work was supported by The Pew Scholars Program in the Biomedical Sciences and by National Institutes of Health grants GM079320 and GM100083 to D.R. Sherwood.

Submitted: 23 January 2013
Accepted: 1 May 2013

References

Artym, V.V., Y. Zhang, F. Seillier-Moiseiwitsch, K.M. Yamada, and S.C. Mueller. 2006. Dynamic interactions of cortactin and membrane type 1 matrix metalloproteinase at invadopodia: defining the stages of invadopodia formation and function. *Cancer Res.* 66:3034–3043. http://dx.doi.org/10.1158/0008-5472.CAN-05-2177

Ayala, I., M. Baldassarre, G. Giacchetti, G. Caldieri, S. Tetè, A. Luini, and R. Buccione. 2008. Multiple regulatory inputs converge on cortactin to control invadopodia biogenesis and extracellular matrix degradation. *J. Cell Sci.* 121:369–378. http://dx.doi.org/10.1242/jcs.008037

Brenner, S. 1974. The genetics of *Caenorhabditis elegans*. *Genetics*. 77:71–94.

Castets, M., L. Broutier, Y. Molin, M. Brevet, G. Chazot, N. Gadot, A. Paquet, L. Mazelin, L. Jarrosson-Wuilleme, J.Y. Scoazec, et al. 2012. DCC constrains tumour progression via its dependence receptor activity. *Nature*. 482:534–537. http://dx.doi.org/10.1038/nature10708

Chen, W.T. 1989. Proteolytic activity of specialized surface protrusions formed at rosette contact sites of transformed cells. *J. Exp. Zool.* 251:167–185. http://dx.doi.org/10.1002/jez.1402510206

David-Pfeuty, T., and S.J. Singer. 1980. Altered distributions of the cytoskeletal proteins vinculin and alpha-actinin in cultured fibroblasts transformed by Rous sarcoma virus. *Proc. Natl. Acad. Sci. USA*. 77:6687–6691. http://dx.doi.org/10.1073/pnas.77.11.6687

Destaing, O., E. Planus, D. Bouvard, C. Oddou, C. Badowski, V. Bossy, A. Raducanu, B. Fourcade, C. Albiges-Rizo, and M.R. Block. 2010. β1A integrin is a master regulator of invadosome organization and function. *Mol. Biol. Cell*. 21:4108–4119. http://dx.doi.org/10.1091/mbc.E10-07-0580

Dumartin, L., C. Quemener, H. Laklai, J. Herbert, R. Bicknell, C. Bousquet, S. Pyronnet, V. Castronovo, M.K. Schilling, A. Bikfalvi, and M. Hagedorn. 2010. Netrin-1 mediates early events in pancreatic adenocarcinoma progression, acting on tumor and endothelial cells. *Gastroenterology*. 138:1595–1606: 1606: e1–e8. http://dx.doi.org/10.1053/j.gastro.2009.12.061

Fitamant, J., C. Guenebeaud, M.M. Coissieux, C. Guix, I. Treilleux, J.Y. Scoazec, T. Bachelot, A. Bernet, and P. Mehlen. 2008. Netrin-1 expression confers a selective advantage for tumor cell survival in metastatic breast cancer. *Proc. Natl. Acad. Sci. USA*. 105:4850–4855. http://dx.doi.org/10.1073/pnas.0709810105

Garbisa, S., K. Kniska, K. Tryggvason, C. Foltz, and L.A. Liotta. 1980. Quantitation of basement membrane collagen degradation by living tumor cells in vitro. *Cancer Lett.* 9:359–366. http://dx.doi.org/10.1016/0304-3835(80)90030-0

Gurskaya, N.G., V.V. Verkhusha, A.S. Shcheglov, D.B. Staroverov, T.V. Chepurnykh, A.F. Fradkov, S. Lukyanov, and K.A. Lukyanov. 2006. Engineering of a monomeric green-to-red photoactivatable fluorescent protein induced by blue light. *Nat. Biotechnol.* 24:461–465. http://dx.doi.org/10.1038/nbt1191

Hagedorn, E.J., and D.R. Sherwood. 2011. Cell invasion through basement membrane: the anchor cell breaches the barrier. *Curr. Opin. Cell Biol.* 23:589–596. http://dx.doi.org/10.1016/j.ceb.2011.05.002

Hagedorn, E.J., H. Yashiro, J.W. Ziel, S. Ihara, Z. Wang, and D.R. Sherwood. 2009. Integrin acts upstream of netrin signaling to regulate formation of the anchor cell's invasive membrane in *C. elegans*. *Dev. Cell*. 17:187–198. http://dx.doi.org/10.1016/j.devcel.2009.06.006

Downloaded from on June 27, 2017

Published June 10, 2013

Heissig, B., K. Hattori, M. Friedrich, S. Rafii, and Z. Werb. 2003. Angiogenesis: vascular remodeling of the extracellular matrix involves metalloproteinases. *Curr. Opin. Hematol.* 10:136–141. http://dx.doi.org/10.1097/00062752-200303000-00007

Hoshino, D., J. Jourquin, S.W. Emmons, T. Miller, M. Goldgof, K. Costello, D.R. Tyson, B. Brown, Y. Lu, N.K. Prasad, et al. 2012. Network analysis of the focal adhesion to invadopodia transition identifies a PI3K-PKCα invasive signaling axis. *Sci. Signal.* 5:ra66. http://dx.doi.org/10.1126/scisignal.2002964

Hotary, K., X.Y. Li, E. Allen, S.L. Stevens, and S.J. Weiss. 2006. A cancer cell metalloprotease triad regulates the basement membrane transmigration program. *Genes Dev.* 20:2673–2686. http://dx.doi.org/10.1101/gad.1451806

Hughes, S.M., and H.M. Blau. 1990. Migration of myoblasts across basal lamina during skeletal muscle development. *Nature*. 345:350–353. http://dx.doi.org/10.1038/345350a0

Ihara, S., E.J. Hagedorn, M.A. Morrissey, Q. Chi, F. Motegi, J.M. Kramer, and D.R. Sherwood. 2011. Basement membrane sliding and targeted adhesion remodels tissue boundaries during uterine-vulval attachment in *Caenorhabditis elegans*. *Nat. Cell Biol.* 13:641–651. http://dx.doi.org/10.1038/ncb2233

Kalluri, R. 2003. Basement membranes: structure, assembly and role in tumour angiogenesis. *Nat. Rev. Cancer*. 3:422–433. http://dx.doi.org/10.1038/nrc1094

Kaufmann, S., S. Kuphal, T. Schubert, and A.K. Bosserhoff. 2009. Functional implication of Netrin expression in malignant melanoma. *Cell. Oncol.* 31:415–422.

Klemke, R.L. 2012. Trespassing cancer cells: 'fingerprinting' invasive protrusions reveals metastatic culprits. *Curr. Opin. Cell Biol.* 24:662–669. http://dx.doi.org/10.1016/j.ceb.2012.08.005

Krimpenfort, P., J.Y. Song, N. Proost, J. Zevenhoven, J. Jonkers, and A. Berns. 2012. Deleted in colorectal carcinoma suppresses metastasis in p53-deficient mammary tumours. *Nature*. 482:538–541. http://dx.doi.org/10.1038/nature10790

Lai Wing Sun, K., J.P. Correia, and T.E. Kennedy. 2011. Netrins: versatile extracellular cues with diverse functions. *Development*. 138:2153–2169. http://dx.doi.org/10.1242/dev.044529

Linder, S., C. Wiesner, and M. Himmel. 2011. Degrading devices: invadosomes in proteolytic cell invasion. *Annu. Rev. Cell Dev. Biol.* 27:185–211. http://dx.doi.org/10.1146/annurev-cellbio-092910-154216

Madsen, C.D., and E. Sahai. 2010. Cancer dissemination—lessons from leukocytes. *Dev. Cell*. 19:13–26. http://dx.doi.org/10.1016/j.devcel.2010.06.013

Murphy, D.A., and S.A. Courtneidge. 2011. The 'ins' and 'outs' of podosomes and invadopodia: characteristics, formation and function. *Nat. Rev. Mol. Cell Biol.* 12:413–426. http://dx.doi.org/10.1038/nrm3141

Nakahara, H., T. Otani, T. Sasaki, Y. Miura, Y. Takai, and M. Kogo. 2003. Involvement of Cdc42 and Rac small G proteins in invadopodia formation of RPMI7951 cells. *Genes Cells*. 8:1019–1027. http://dx.doi.org/10.1111/j.1365-2443.2003.00695.x

Nakaya, Y., E.W. Sukowati, Y. Wu, and G. Sheng. 2008. RhoA and microtubule dynamics control cell-basement membrane interaction in EMT during gastrulation. *Nat. Cell Biol.* 10:765–775. http://dx.doi.org/10.1038/ncb1739

Overall, C.M., and O. Kleifeld. 2006. Validating matrix metalloproteinases as drug targets and anti-targets for cancer therapy. *Nat. Rev. Cancer*. 6:227–239. http://dx.doi.org/10.1038/nrc1821

Page-McCaw, A., A.J. Ewald, and Z. Werb. 2007. Matrix metalloproteinases and the regulation of tissue remodelling. *Nat. Rev. Mol. Cell Biol.* 8:221–233. http://dx.doi.org/10.1038/nrm2125

Philippar, U., E.T. Roussos, M. Oser, H. Yamaguchi, H.D. Kim, S. Giampieri, Y. Wang, S. Goswami, J.B. Wyckoff, D.A. Lauffenburger, et al. 2008. A Mena invasion isoform potentiates EGF-induced carcinoma cell invasion and metastasis. *Dev. Cell*. 15:813–828. http://dx.doi.org/10.1016/j.devcel.2008.09.003

Poelmann, R.E., A.C. Gittenberger-de Groot, M.M. Mentink, B. Delpech, N. Girard, and B. Christ. 1990. The extracellular matrix during neural crest formation and migration in rat embryos. *Anat. Embryol. (Berl.)*. 182:29–39. http://dx.doi.org/10.1007/BF00187525

Quinn, C.C., D.S. Pfeil, and W.G. Wadsworth. 2008. CED-10/Rac1 mediates axon guidance by regulating the asymmetric distribution of MIG-10/lamellipodin. *Curr. Biol.* 18:808–813. http://dx.doi.org/10.1016/j.cub.2008.04.050

Rabinovitz, I., I.K. Gipson, and A.M. Mercurio. 2001. Traction forces mediated by alpha6beta4 integrin: implications for basement membrane organization and tumor invasion. *Mol. Biol. Cell*. 12:4030–4043.

Ramesh, G., A. Berg, and C. Jayakumar. 2011. Plasma netrin-1 is a diagnostic biomarker of human cancers. *Biomarkers*. 16:172–180. http://dx.doi.org/10.3109/1354750X.2010.541564

Rodrigues, S., O. De Wever, E. Bruyneel, R.J. Rooney, and C. Gespach. 2007. Opposing roles of netrin-1 and the dependence receptor DCC in cancer cell invasion, tumor growth and metastasis. *Oncogene*. 26:5615–5625. http://dx.doi.org/10.1038/sj.onc.1210347

Rowe, R.G., and S.J. Weiss. 2008. Breaching the basement membrane: who, when and how? *Trends Cell Biol.* 18:560–574. http://dx.doi.org/10.1016/j.tcb.2008.08.007

Saltel, F., T. Daubon, A. Juin, I.E. Ganuza, V. Veillat, and E. Génot. 2011. Invadosomes: intriguing structures with promise. *Eur. J. Cell Biol.* 90:100–107. http://dx.doi.org/10.1016/j.ejcb.2010.05.011

Sato, Y., T. Higuchi, S. Yoshioka, K. Tatsumi, H. Fujiwara, and S. Fujii. 2003. Trophoblasts acquire a chemokine receptor, CCR1, as they differentiate towards invasive phenotype. *Development*. 130:5519–5532. http://dx.doi.org/10.1242/dev.00729

Schoumacher, M., R.D. Goldman, D. Louvard, and D.M. Vignjevic. 2010. Actin, microtubules, and vimentin intermediate filaments cooperate for elongation of invadopodia. *J. Cell Biol.* 189:541–556. http://dx.doi.org/10.1083/jcb.200909113

Seiler, C., G. Davuluri, J. Abrams, F.J. Byfield, P.A. Janmey, and M. Pack. 2012. Smooth muscle tension induces invasive remodeling of the zebrafish intestine. *PLoS Biol.* 10:e1001386. http://dx.doi.org/10.1371/journal.pbio.1001386

Shaye, D.D., and I. Greenwald. 2011. OrthoList: a compendium of *C. elegans* genes with human orthologs. *PLoS ONE*. 6:e20085. http://dx.doi.org/10.1371/journal.pone.0020085

Sherwood, D.R., and P.W. Sternberg. 2003. Anchor cell invasion into the vulval epithelium in *C. elegans*. *Dev. Cell*. 5:21–31. http://dx.doi.org/10.1016/S1534-5807(03)00168-0

Sherwood, D.R., J.A. Butler, J.M. Kramer, and P.W. Sternberg. 2005. FOS-1 promotes basement-membrane removal during anchor-cell invasion in *C. elegans*. *Cell*. 121:951–962. http://dx.doi.org/10.1016/j.cell.2005.03.031

Shimizu, A., H. Nakayama, P. Wang, C. Konig, T. Akino, J. Sandlund, S. Coma, J.E. Italiano, A. Mammoto, D.R. Bielenberg, and M. Klagsbrun. 2012. Netrin-1 promotes glioblastoma cell invasiveness and angiogenesis by multiple pathways including activation of RhoA, cathepsin B and cAMP-response element-binding protein. *J. Biol. Chem.* 288:2210–2222. http://dx.doi.org/10.1074/jbc.M112.397398

Valastyan, S., and R.A. Weinberg. 2011. Tumor metastasis: molecular insights and evolving paradigms. *Cell*. 147:275–292. http://dx.doi.org/10.1016/j.cell.2011.09.024

VanZomeren-Dohm, A., J. Sarro, E. Flannery, and M. Duman-Scheel. 2011. The *Drosophila* Netrin receptor frazzled/DCC functions as an invasive tumor suppressor. *BMC Dev. Biol.* 11:41. http://dx.doi.org/10.1186/1471-213X-11-41

Wang, S., M.B. Voisin, K.Y. Larbi, J. Dangerfield, C. Scheiermann, M. Tran, P.H. Maxwell, L. Sorokin, and S. Nourshargh. 2006. Venular basement membranes contain specific matrix protein low expression regions that act as exit points for emigrating neutrophils. *J. Exp. Med.* 203:1519–1532. http://dx.doi.org/10.1084/jem.20051210

Wilson, B.D., M. Ii, K.W. Park, A. Suli, L.K. Sorensen, F. Larrieu-Lahargue, L.D. Urness, W. Suh, J. Asai, G.A. Kock, et al. 2006. Netrins promote developmental and therapeutic angiogenesis. *Science*. 313:640–644. http://dx.doi.org/10.1126/science.1124704

Xu, J., D. Rodriguez, E. Petitclerc, J.J. Kim, M. Hangai, Y.S. Moon, G.E. Davis, and P.C. Brooks. 2001. Proteolytic exposure of a cryptic site within collagen type IV is required for angiogenesis and tumor growth in vivo. *J. Cell Biol.* 154:1069–1079. (published erratum appears in *J. Cell Biol.* 2001. 155:859) http://dx.doi.org/10.1083/jcb.200103111

Yamaguchi, H., S. Yoshida, E. Muroi, M. Kawamura, Z. Kouchi, Y. Nakamura, R. Sakai, and K. Fukami. 2010. Phosphatidylinositol 4,5-bisphosphate and PIP5-kinase Ialpha are required for invadopodia formation in human breast cancer cells. *Cancer Sci.* 101:1632–1638. http://dx.doi.org/10.1111/j.1349-7006.2010.01574.x

Ziel, J.W., E.J. Hagedorn, A. Audhya, and D.R. Sherwood. 2009. UNC-6 (netrin) orients the invasive membrane of the anchor cell in *C. elegans*. *Nat. Cell Biol.* 11:183–189. http://dx.doi.org/10.1038/ncb1825

Downloaded from on June 27, 2017

Hagedorn et al., http://www.jcb.org/cgi/content/full/jcb.201301091/DC1

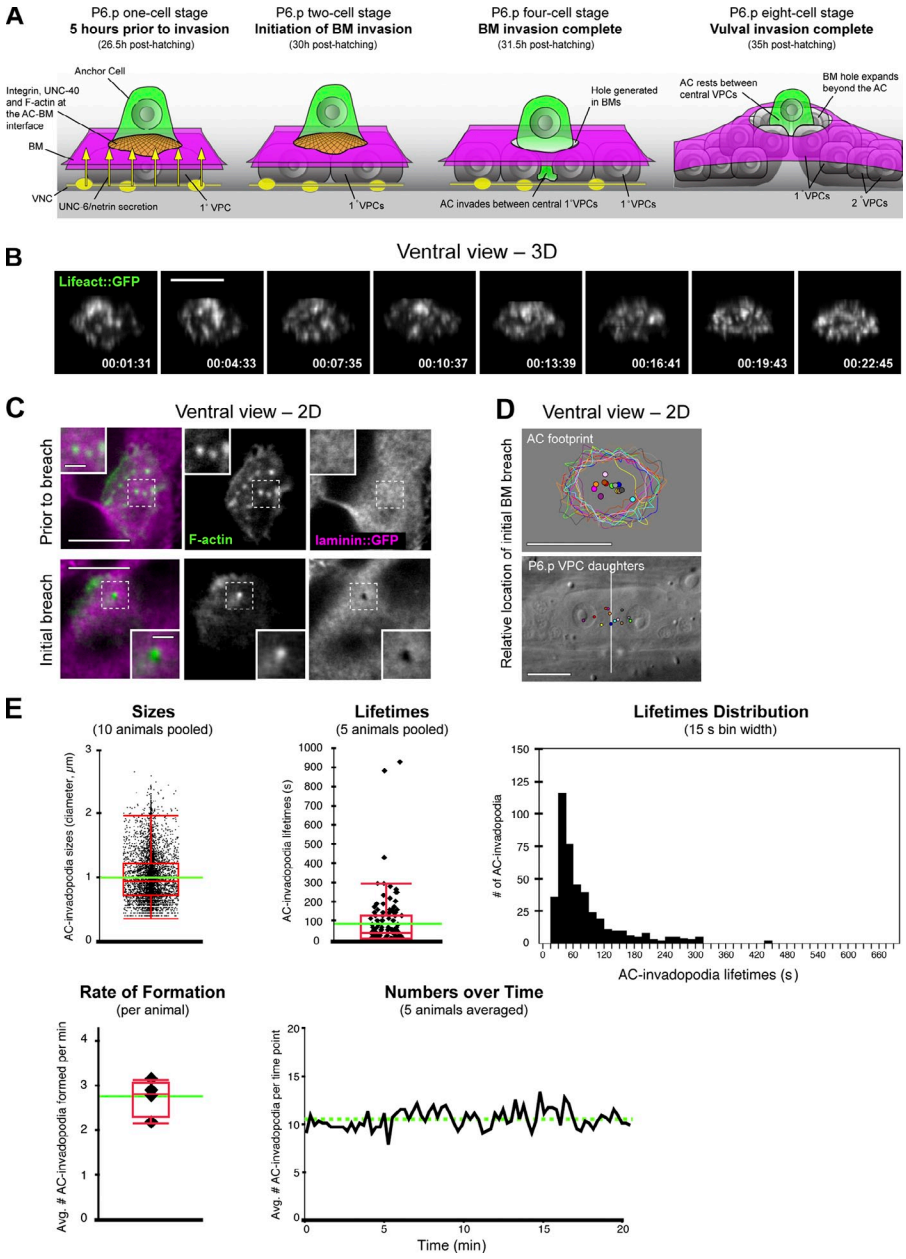

Figure S1. **AC-invadopodia breach the basement membrane.** (A) Schematic diagram depicts four developmental time points over the course of AC invasion in *C. elegans* (times shown are after hatching at 20°C). 5 h before invasion, at the P6.p one-cell stage, the integrin receptor INA-1/PAT-3 and the netrin receptor UNC-40 (DCC) localize to the invasive cell membrane and regulate a polarized F-actin–rich membrane domain (orange) within the AC (green) at the basement membrane (BM) interface (magenta). AC invasion initiates at the P6.p two-cell stage and by the P6.p four-cell stage the AC clears a large gap in the basement membrane and moves between the central P6.p vulval cells. By the P6.p eight-cell stage, the invaginating vulval cells have expanded the gap in the basement membrane beyond the AC, where it then stabilizes in its position. At this time the AC is situated at the apex of the vulva between the central vulval cells. (B) A ventral view time series of an AC-specific Lifeact::GFP probe (*cdh-3 > Lifeact::GFP*), an alternative F-actin marker, reveals dynamic F-actin–rich invadopodia along the invasive cell membrane of the AC. Images were acquired using a lateral view of the animal and then rotated on the z axis, resulting in some cropping of the most proximal part of the image (top of images shown). Bar, 5 µm. (C) Ventral view images show F-actin–rich AC-invadopodia (middle, expressing *cdh-3 >* mCherry::moeABD) in relation to the basement membrane (left, overlay; right, viewed with laminin::GFP). AC-invadopodia form before breach (top, dashed boxes, insets) and occupy the initial breach site (bottom, dashed boxes, insets). Bars: (main images) 5 µm; (insets) 1 µm. (D) The diagrams depict the location of the initial basement membrane breach (spots) relative to the footprint of the AC (top, outlines) and underlying P6.p vulval cells (bottom, vertical white line marks the interface of the central vulval cells; *n* = 13 animals). Each color represents the same animal. (E) The graphs show quantitative data of wild-type AC-invadopodia in the hour preceding basement membrane invasion. Green lines denote population means for measurements of size (1.00 µm; *n* = 8,182 structures), lifetime (1.13 min; *n* = 729 structures), rate of formation (2.8 structures per minute), and numbers over time (11 structures); red boxes show the interquartile range and whiskers show 1.5 × interquartile range. The same data are shown in the lifetimes and lifetimes distribution graph.

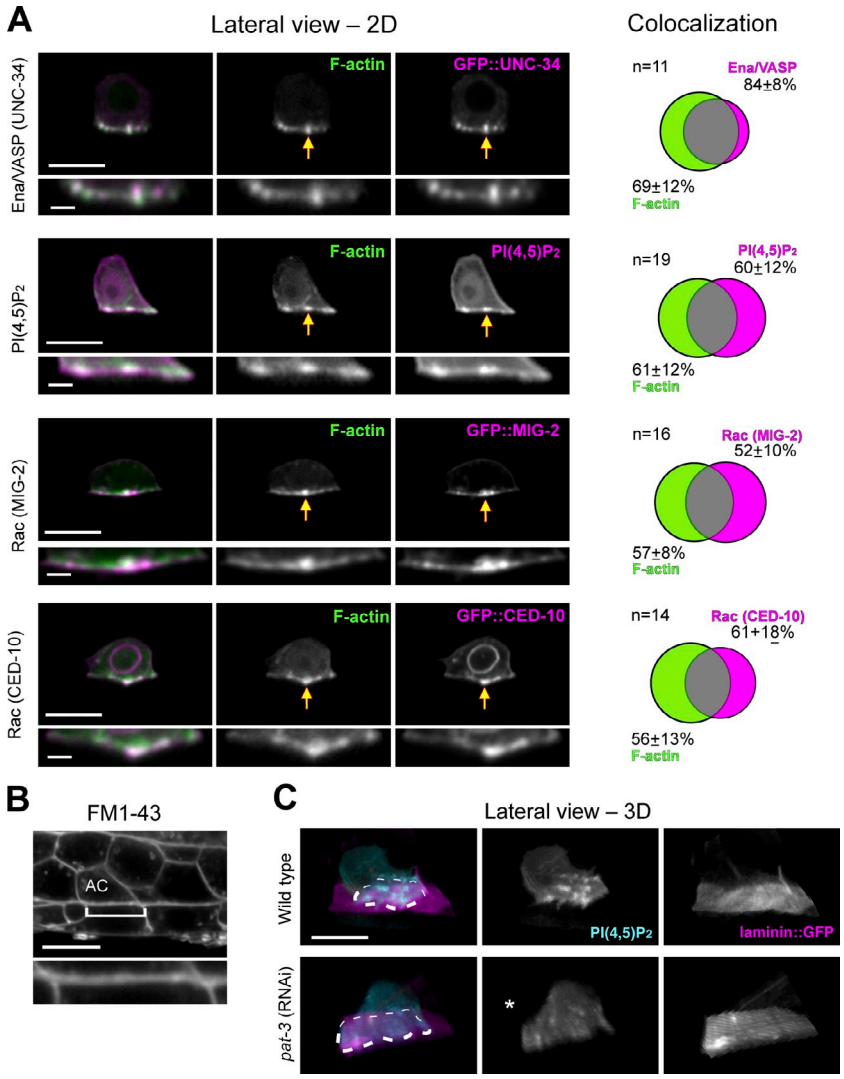

Figure S2. **AC-invadopodia are enriched in actin regulators and are dependent on integrin.** (A) Lateral view images show ACs coexpressing the F-actin marker *cdh-3* > mCherry::moeABD (green in overlays) and one of four GFP-tagged proteins (GFP::UNC-34, mCherry::PLCδ^{PH} [PI(4,5)P_2], GFP::MIG-2, and GFP::CED-10; magenta in overlays). Arrows point to colocalization at F-actin structures; insets show magnification of the invasive cell membrane. Venn diagrams (right) display the percentage of total volume colocalized for each protein. The mean percent overlap ± SD is reported. Bars: (main images) 5 µm; (insets) 1 µm. (B) The vital dye FM1-43, which labels the outer leaflet of the plasma membrane, was not enriched at invadopodia structures at the AC–basement membrane interface (bracket). (C) Images show 3D reconstructions of confocal z-stacks rotated forward. The AC is expressing the PI(4,5)P_2 marker *cdh-3* > mCherry::PLCδ^{PH} (cyan). The basement membrane is visualized with laminin::GFP (magenta). In wild-type animals (top) many invadopodia are present along the invasive cell membrane of the AC (outlined with a dashed circle in the overlay). RNAi knockdown of *pat-3* (bottom), the β-subunit of the integrin heterodimer INA-1/PAT-3, resulted in a dramatic reduction in invadopodia formation (asterisk; similar results observed in eight animals).

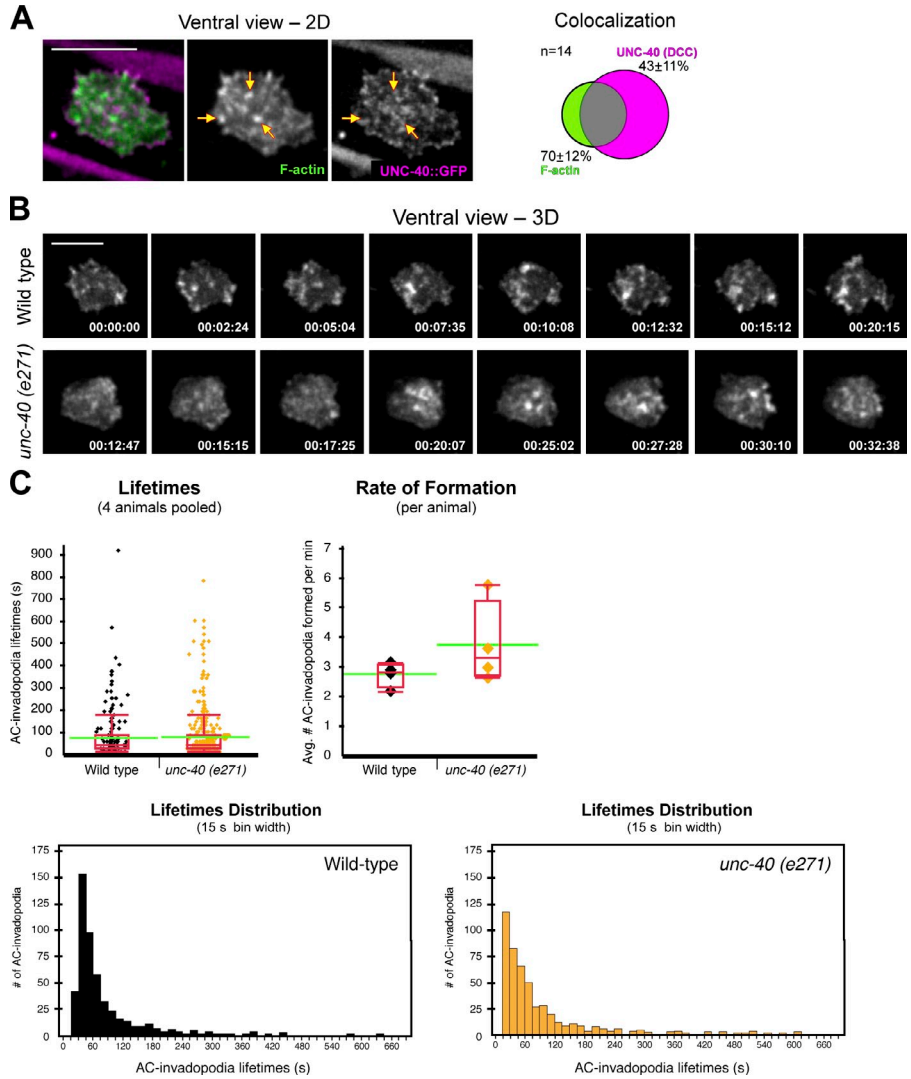

Figure S3. **UNC-40 does not localize to invadopodia or regulate their dynamics.** (A) Lateral view images show an AC coexpressing the F-actin marker *cdh-3* > mCherry::moeABD (green in overlay) and UNC-40::GFP (magenta). Arrows highlight F-actin–rich AC-invadopodia that lack specific enrichment of UNC-40::GFP. Venn diagram (right) shows the percentage of total volume colocalized for UNC-40 and F-actin. The mean percent overlap ± SD is reported. (B) Ventral view time series show similar invadopodia dynamics (viewed with *cdh-3* > mCherry::moeABD) in wild type (top) and *unc-40* mutants (bottom). Bars, 5 µm. (C) Graphs show quantitative analysis of invadopodia lifetimes and rate of formation in wild-type animals and in *unc-40 (e271)* mutants. Red boxes mark the interquartile range and whiskers show 1.5 × interquartile range. Green lines denote population means for measurements. Wild-type invadopodia had mean lifetimes of 84 s and formed at a mean rate of 2.8 structures per minute (n = 309 structures from four animals). In *unc-40* mutants, invadopodia had mean lifetimes of 81 s and formed at a mean rate of 3.8 structures per minute (n = 473 structures from four animals). No statistical differences were observed ($P > 0.05$, Wilcoxon rank-sum test). The same data for wild type and *unc-40 (e271)* is reported in the lifetimes graph (top left) and lifetimes distribution graphs (bottom). The error bars represent the SEM.

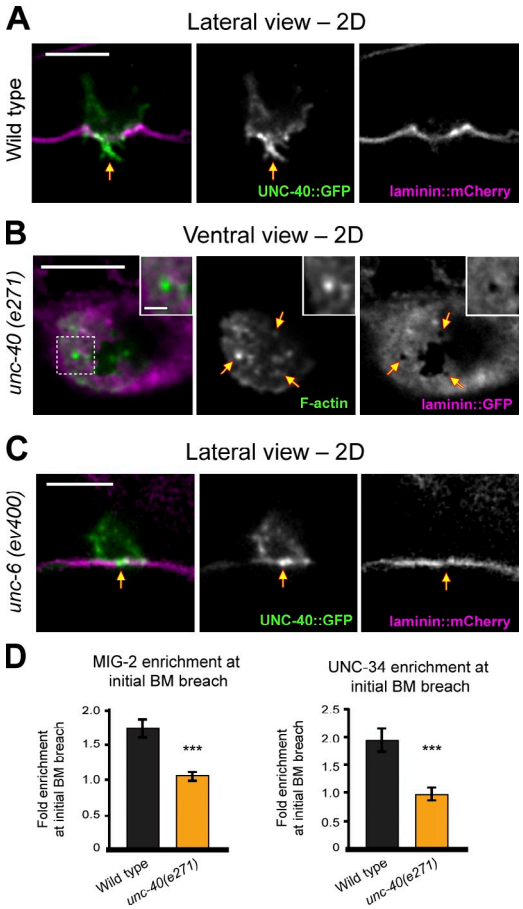

Figure S4. **UNC-40 localization and regulation of invadopodia breaching.** (A) Lateral view images show an AC coexpressing UNC-40::GFP (green in overlay) and laminin::mCherry (labeling the basement membrane; magenta). Arrows highlight UNC-40::GFP enriched in the invasive protrusion. (B) Ventral view images show AC-invadopodia (viewed with *cdh-3* > mCherry::moeABD; green) and the basement membrane component laminin::GFP (magenta) in an *unc-40* mutant animal. Invadopodia occupy multiple breaches in the basement membrane (arrows; dashed box corresponds to inset). Bars: (main images) 5 µm; (insets) 1 µm. (C) Lateral view images show an AC coexpressing UNC-40::GFP (green in overlay) and the basement membrane component laminin::mCherry (magenta) in an *unc-6* mutant animal. UNC-40::GFP localizes to the site of basement membrane breach (arrows) in *unc-6* mutants to a similar extent as wild-type animals (2.21-fold enrichment at breach relative to the invasive cell membrane in *unc-6* mutants and 2.48-fold enrichment in wild-type animals; $n = 10$ animals examined for each; $P > 0.43$, Student's *t* test). (D) Graphs show the fold enrichment of MIG-2 and UNC-34 at the initial basement membrane breach (relative to the rest of the invasive membrane). The fold enrichment of MIG-2 and UNC-34 at the initial basement membrane breach was reduced in *unc-40 (e271)* (MIG-2 = 1.07-fold; UNC-34 = 0.97-fold) compared with wild type (MIG-2 = 1.74-fold; UNC-34 = 1.93-fold; $n \geq 10$ animals each marker/genotype; $P < 0.001$, Student's *t* test). The error bars represent the SEM.

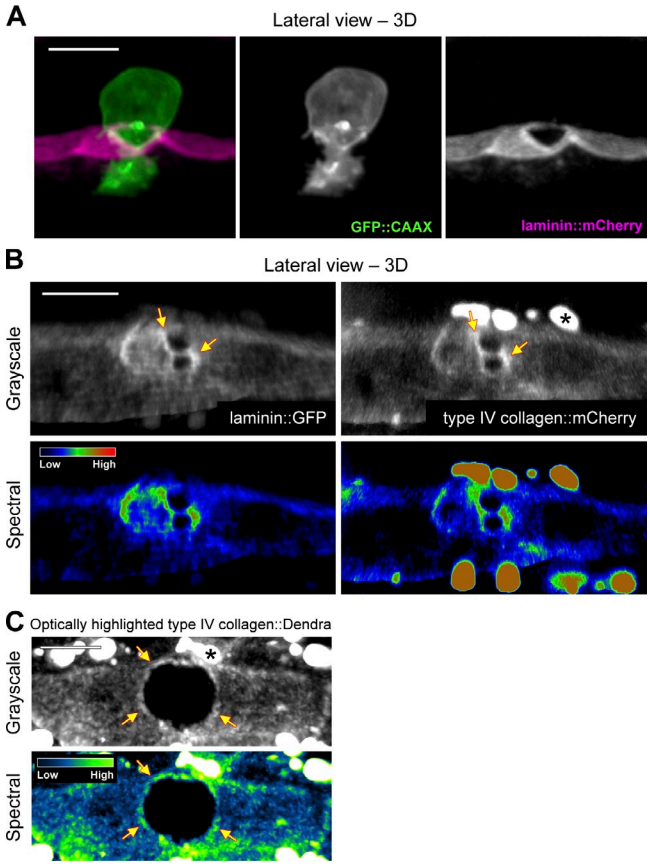

Figure S5. **The basement membrane is physically displaced during invasion.** (A) Images show how the invasive protrusion from the AC (visualized with GFP::CAAX membrane marker; green in overlay) maintains continuous contact with the edges of the expanding basement membrane gap (magenta). (B) Images of an animal coexpressing laminin::GFP (left) and type IV collagen::mCherry (right) show that both basement membrane components accumulate at the edge of the expanding basement membrane gap (arrows; grayscale above and spectral representation of fluorescence intensity below). Asterisks in B and C mark large intracellular accumulations of type IV collagen in neighboring muscle cells. (C) Images show accumulation of displaced optically highlighted type IV collagen::Dendra at the edges of the expanding basement membrane gap (arrows; grayscale above and spectral representation of fluorescence intensity below; see Fig. 6 B for experimental details). Bars, 5 µm.

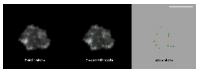

Video 1. **AC-invadopodia turn over dynamically before basement membrane breaching.** Ventral view time-lapse shows dynamic F-actin–rich AC-invadopodia (visualized with the F-actin probe *cdh-3* > mCherry::moeABD; left) prior to invasion. Images were acquired using a spinning disc confocal microscope (CSU-10 scan head; Yokogawa) mounted on a microscope (AxioImager; Carl Zeiss). Spot tracking analysis was performed in IMARIS 7.4 (Bitplane, Inc.) to quantify invadopodia dynamics (reported in Figs. S1 E and S3 C). A 60-min time-lapse is shown with time points acquired every 15 s. A projection of eight confocal z-sections (step size of 0.5 µm) is shown. The video plays at 10 frames per second. Bar, 5 µm. This video corresponds to the animal shown in Fig. 1 B.

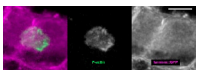

Video 2. **An AC-invadopodium presages and then occupies the site of basement membrane breach.** Ventral view time-lapse shows an AC-invadopodium (visualized with *cdh-3* > mCherry::moeABD in green) that presages (center, arrowhead) and then occupies the basement membrane breach (right, arrowhead). Images were acquired using a spinning disc confocal microscope (CSU-10 scan head; Yokogawa) mounted on a microscope (AxioImager; Carl Zeiss). A 30-min time-lapse is shown with time points acquired every 15 s. A projection of eight confocal z-sections (step size of 0.5 µm) is shown. Bar, 5 µm. This video corresponds to the animal shown in Fig. 1 E.

Video 3. **Invasive protrusion growth during basement membrane transmigration.** An AC is shown just after breaching the basement membrane (3D lateral view rotated forward). The video shows the AC's invasive protrusion (cyan) expanding through the basement membrane breach (magenta) and into the vulval tissue. The AC's cell membrane is visualized with a PI(4,5)P2 probe (*cdh-3* > mCherry::PLCδ^{PH}) and the basement membrane with laminin::GFP. Images were acquired using a spinning disc confocal microscope (CSU-10 scan head; Yokogawa) mounted on a microscope (AxioImager; Carl Zeiss). A 60-min time-lapse is shown with time points acquired every minute. A projection of seven confocal z-sections (step size of 1 µm) is shown. Bar, 5 µm. This video corresponds to the animal shown in Fig. 2 A.

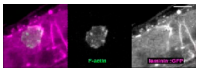

Video 4. **The invadopodia-to-invasive protrusion transition.** Ventral view time-lapse shows the transition between dynamic AC-invadopodia (visualized with the F-actin probe *cdh-3* > mCherry::moeABD in green) and the formation of a stable protrusion at the site of basement membrane breaching (visualized with laminin::GFP in magenta). Halfway through the video, AC-invadopodia cease to form along the remainder of the AC–basement membrane interface (overlay on left), as an invasive protrusion expands rapidly through the basement membrane and the corresponding breach widens radially. Images were acquired using a spinning disc confocal microscope (CSU-10 scan head; Yokogawa) mounted on a microscope (AxioImager; Carl Zeiss). A 60-min time-lapse is shown with time points acquired every 15 s. A projection of eight confocal z-sections (step size of 0.5 µm) is shown. Video is played at 20 frames per second. Bar, 5 µm.

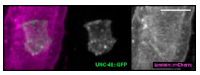

Video 5. **UNC-40::GFP enriches at the basement membrane breach.** Ventral view time-lapse shows UNC-40::GFP (green) enriching at the site of basement membrane breach (visualized with laminin::mCherry in magenta). Images were acquired using a spinning disc confocal microscope (CSU-10 scan head; Yokogawa) mounted on a microscope (AxioImager; Carl Zeiss). A 60-min time-lapse is shown with time points acquired every 2 min. A projection of eight confocal z-sections (step size of 0.5 µm) is shown. Bar, 5 µm. This video corresponds to the animal shown in Fig. 3 B.

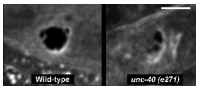

Video 6. **UNC-40 accelerates basement membrane gap opening.** Ventral view time-lapses show similarly sized basement membrane gaps (visualized with laminin::GFP) in a wild-type and an *unc-40* mutant animal. The basement membrane breach in the *unc-40* mutant animal opens at half the rate of the wild-type animals (for quantification see Fig. 4 F). Images were acquired using a spinning disc confocal microscope (CSU-10 scan head; Yokogawa) mounted on a microscope (AxioImager; Carl Zeiss). A 60-min time-lapse is shown with time points acquired every 2 min. A projection of eight confocal z-sections (step size of 0.5 µm) is shown. Bar, 5 µm. This video corresponds to the animals shown in Fig. 4 E.

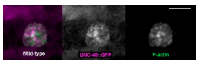

Video 7. **F-actin formation is focused at sites of UNC-40::GFP enrichment.** Ventral view time-lapse reveals recurrent F-actin formation (visualized with *cdh-3* > mCherry::moeABD in green) at the site-stable UNC-40::GFP (magenta) enrichment. Images were acquired using a spinning disc confocal microscope (CSU-10 scan head; Yokogawa) mounted on a microscope (AxioImager; Carl Zeiss)). A 60-min time-lapse is shown with time points acquired every 15 s. A projection of eight confocal z-sections (step size of 0.5 µm) is shown. Bar, 5 µm. This video corresponds to the animal and time-lapse summation shown in Fig. 5 B.

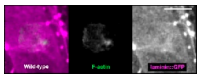

Video 8. **F-actin formation is focused at the basement membrane breach in wild-type animals.** Ventral view time-lapse shows recurrent F-actin formation (visualized with *cdh-3* > mCherry::moeABD in green) at the site of basement membrane breach (visualized with laminin::GFP in magenta) in a wild-type animal. Images were acquired using a spinning disc confocal microscope (CSU-10 scan head; Yokogawa) mounted on a microscope (AxioImager; Carl Zeiss)). A 60-min time-lapse is shown with time points acquired every 15 s. A projection of eight confocal z-sections (step size of 0.5 µm) is shown. Bar, 5 µm. This video corresponds to the wild-type animal and time-lapse summation shown in Fig. 5 C.

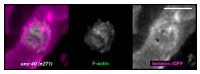

Video 9. **F-actin formation is not focused at basement membrane breaches in *unc-40* mutants.** Ventral view time-lapse demonstrates that dynamic F-actin formation (visualized with *cdh-3* > mCherry::moeABD in green) is not tightly correlated with the sites of basement membrane breach (visualized with laminin::GFP in magenta) in an *unc-40 (e271)* mutant animal. Images were acquired using a spinning disc confocal microscope (CSU-10 scan head; Yokogawa) mounted on a microscope (AxioImager; Carl Zeiss). A 60-min time-lapse is shown with time points acquired every 15 s. A projection of eight confocal z-sections (step size of 0.5 µm) is shown. Bar, 5 µm. This video corresponds to the *unc-40 (e271)* animal and time-lapse summation shown in Fig. 5 C.

Table S1. **Primer sequences and templates used for all PCR fusions generated**

Primer sequence	Primer type	Amplicon	Template
5′-TAATgTgAgTTAgCTCACTCATTAgg-3′	forward	*cdh-3* > promoter	pPD107.94/mk62-63
5′-AACgATggATACgCTAACAACTTgg-3′	forward nested	*cdh-3* > promoter	pPD107.94/mk62-63
5′-TTTCTgAgCTCggTACCCTCCAAg-3′	reverse	*cdh-3* > promoter	pPD107.94/mk62-63
5′-ATgAgTAAAggAgAAgAACTTTTC-3′	forward	*GFP*	pPD95_81
5′-TTTgTATAgTTCATCCATgCCATg-3′	reverse	*GFP*	pPD95_81
5′-CTTggAgggTACCgAgCTCAgAAAATggATACgCTAACAACTTgg-3′	*cdh-3* extension, forward	*Lifeact::GFP*	pJWZ73
5′-TTTCACCAgCgTTTCTgggTgAgC-3′	reverse	*Lifeact::GFP*	pJWZ73
5′-TggTgCACTCTCAgTACAATCTgC-3′	reverse nested	*Lifeact::GFP*	pJWZ73
5′ ACtATAgggCgAATTgggTACCgg-3′	forward	*GFP::PLCδ^{PH}*	*pBsSK-GFP-PLCδ^{PH}*
5′-CTTggAgggTACCgAgCTCAgAAAATggTCTCAAAgggTgAAgAAgAT-3′	*cdh-3* extension, forward nested	*GFP::PLCδ^{PH}*	*pBsSK-GFP-PLCδ^{PH}*
5′-TTACTTCTgCCgCTggTCCATggA-3′	reverse	*GFP::PLCδ^{PH}*	*pBsSK-GFP-PLCδ^{PH}*
5′-ATTACACATggCATggATgAACTAATgTCTTCACCgTCgAggCAgATC-3′	*gfp* extension, forward	*MIG-2*	N2 genomic DNA
5′-AAAAACgACTCAATAggTgAgCgC-3′	reverse	*MIG-2*	N2 genomic DNA
5′-gTTgCTCTAAAAACCCgATCTTCC-3′	reverse nested	*MIG-2*	N2 genomic DNA
5′-ATTACACATggCATggATgAACTAATgCAAgCgATCAAATgTgTCgTC-3′	*gfp* extension, forward	*CED-10*	N2 genomic DNA
5′-TTCTATCAAATggAAgCACAgCgg-3′	reverse	*CED-10*	N2 genomic DNA
5′-TTgATTAgAACTTTTgAATTTCCC-3′	reverse nested	*CED-10*	N2 genomic DNA
5′-CTTggAgggTACCgAgCTCAgAAAATgAgTAAAggAgAAgAACTTTTC-3′	*cdh-3* extension, forward	*GFP::CAAX*	pSA129
5′-TATCAgggTTATTgTCTCATgAgC-3′	reverse	*GFP::CAAX*	pSA129
5′-AgCgAggACAATTCTCATCgTTCg-3′	reverse nested	*GFP::CAAX*	pSA129
5′-TCCATggACCAgCggCAgAAgTAACAACTgAgCgCCggTCgCTACCAT-3′	*PLCδ^{PH}* extension, forward	*unc-54* 3′UTR	pPD95_81
5′-TTTCACCAgCgTTTCTgggTgAgC-3′	reverse	*unc-54* 3′UTR	pPD95_81
5′-gTgCCACCTgACgTCTAAgAAACC-3′	reverse nested	*unc-54* 3′UTR	pPD95_81
5′-TggTgCACTCTCAgTACAATCTgC-3′	reverse nested 2	*unc-54* 3′UTR	pPD95_81

Table S2. **Extrachromosomal arrays and integrated stains generated**

Ex designation	Is designation	PCR fusion created	Injected concentration	Coinjection marker
qyEx234	*qyIs242*	*cdh-3 > Lifeact::GFP*[a]	0.2 ng/ml	unc-119+
qyEx231	*qyIs219*	*cdh-3 > GFP::PLCδ^{PH}* [a,b]	0.01 ng/ml	unc-119+
qyEx232	*qyIs220*	*cdh-3 > GFP::MIG-2*[c,d]	0.2 ng/ml	unc-119+
qyEx233	*qyIs221*	*cdh-3 > GFP::CED-10*[c,d]	0.1 ng/ml	unc-119+
qyEx191	*qyIs166*	*cdh-3 > GFP::CAAX*[a]	0.1 ng/ml	unc-119+

[a]3′UTR from the *unc-54* gene was included at the 3′ end of the construct.
[b]Construct was built using a three-step PCR fusion.
[c]The endogenous 3′ UTR was used.
[d]Coding regions were linked to a *cdh-3 > GFP* amplicon in the last step of the PCR fusion.